American Mineralogist, Volume 107, pages 1736–1751, 2022

Controls on the formation of porphyry Mo deposits: Insights from porphyry (-skarn) Mo deposits in northeastern China

Hegen Ouyang[1,*], John Caulfield[2], Jingwen Mao[1,3], and Ruizhong Hu[4,5]

[1]MNR Key Laboratory of Metallogeny and Mineral Assessment, Institute of Mineral Resources, Chinese Academy of Geological Sciences, Beijing, 100037, China
[2]Central Analytical Research Facility, Queensland University of Technology, Brisbane, 4000 Queensland, Australia
[3]China University of Geosciences, Beijing 100083, China
[4]State Key Laboratory of Ore Deposit Geochemistry, Institute of Geochemistry, Chinese Academy of Sciences, Guiyang, 550081, China
[5]College of Earth and Planetary Sciences, University of Chinese Academy of Sciences, Beijing, 100049, China

Abstract

Porphyry Mo deposits have traditionally been classified into two major classes, arc-related and Climax-type, based on the tectonic setting and chemistry of associated intrusions. Although there is a consensus that porphyry Mo systems were formed by the optimal coincidence of geological processes operating at different scales, it is unclear what key parameter(s) render systems productive and whether the two classes of porphyry Mo deposits are unique in their mode of formation, or if they share fundamentally similar geological processes. These questions are important as a clearer understanding of the optimum conditions for the formation of porphyry Mo deposits is a prerequisite for more efficient exploration.

This contribution presents a detailed assessment of the factors affecting the formation of porphyry Mo deposits through the investigation of barren and mineralized intrusions from the arc-related Songbei-Yangjiazhangzi-Lanjiagou (SYL) ore zone and the Climax-type Hashitu deposit of northeastern China. Our results show that the syn-mineralization intrusions from the SYL ore zone are quite evolved (SiO_2 ~ 75 wt%; Na_2O+K_2O ~ 8.7 wt%) and are characterized by apparent light rare earth element (LREE) enrichments (La_N/Yb_N = 2.7–33.1) and moderate negative Eu anomalies (Eu/Eu* = 0.4–0.7). They show enriched zircon Hf isotopic compositions [$\varepsilon_{Hf}(t)$ = –11.9 to –4.8], indicating their parental magmas were likely derived from an ancient crustal source. Melt inclusions from the SYL syn-mineralization intrusions contain negligible F and Cl. In contrast, Hashitu syn-mineralization intrusions are characterized by weak LREE enrichments (La_N/Yb_N = 2.2–6.9) and strong negative Eu anomalies (Eu/Eu* = 0.02–0.10), with SiO_2 and Na_2O+K_2O contents similar to the SYL syn-mineralization intrusions. They show depleted zircon Hf isotopic compositions [$\varepsilon_{Hf}(t)$ = 3.1–5.0], indicating their parental magmas were likely derived from a juvenile crustal source. Melt inclusions from the Hashitu syn-mineralization intrusions contain up to 0.4 wt% F and 0.03 to 0.09 wt% Cl. However, in both cases, the syn-mineralization intrusions are Mo-poor (1–7 ppm Mo), oxidized (above the quartz-fayalite-magnetite buffer), water-saturated (4.4–7.8 wt% H_2O), and were emplaced at palaeodepths of 3.3 to 8.3 km. These data imply that magma source composition is not a key factor in the formation of porphyry Mo deposits. In contrast, magma oxygen fugacity, water content, and emplacement depth appear to play fundamental roles in the formation of porphyry Mo deposits of both arc-related and Climax-type.

Within individual deposits, no systematic differences between pre- and syn-mineralization intrusions are observed in terms of magma source, fractionation degree, oxygen fugacity, emplacement depth, and volatile and Mo contents. Instead, a crucial apparent difference lies in the geometry of the intrusions, i.e., pre-mineralization intrusions generally occur as flat, ponded bodies, whereas syn-mineralization intrusions commonly develop as small stocks or dikes. Our results, in combination with an examination of other porphyry Mo systems, suggest that the sudden depressurization of magma chambers and subsequent venting of voluminous fluids along focusing structures (such as small stocks or dikes) most likely plays a critical role in the formation of porphyry Mo deposits of both arc-related and Climax-type. The findings of this study indicate that fluid processes in the shallow crust are pivotal for the formation of porphyry Mo deposits and that settings with ideal magmatic-hydrothermal architectures are most likely to develop into productive porphyry Mo systems.

Keywords: Northeastern China, melt inclusions, focused fluid flow, arc-related porphyry Mo deposit, Climax-type porphyry Mo deposit

* E-mail: oyhg1984@163.com.

0003-004X/22/0009–1736$05.00/DOI: https://doi.org/10.2138/am-2021-7665

Introduction

Porphyry Mo deposits, together with porphyry Cu-Mo deposits, represent the most important sources of molybdenum worldwide. They were traditionally classified into two major classes based on the tectonic setting and geochemistry of associated intrusions: (1) Climax-type porphyry Mo deposits associated with fluorine-rich (commonly >1.0 wt% F), highly evolved intrusions in extensional back-arc, post-subduction, or post-collisional settings (Carten et al. 1993; Ludington and Plumlee 2009), and (2) arc-related porphyry Mo deposits associated with fluorine-poor (<0.1 wt% F), differentiated calc-alkaline granitoids in compressional arc-continent subduction and collisional or continent-continent collisional settings (Carten et al. 1993; Taylor et al. 2012). These two classes are considered the product of distinct tectonic settings, which reflect fundamental differences in magma composition and thermal regimes between extensional and compressional environments (Carten et al. 1993; Ludington and Plumlee 2009; Taylor et al. 2012). However, it is still unclear as to whether the two classes of porphyry Mo deposits are unique in their model of ore formation or if they are formed by fundamentally similar geological processes at upper crustal levels (e.g., Stein and Hannah 1985; Carten et al. 1993; Audétat 2010, 2015; Xie et al. 2017; Shu et al. 2019). This is an important question to answer because if they are formed in different ways, predicting the occurrence of porphyry Mo deposits may be difficult. Conversely, if common processes in the upper crust can account for the formation of porphyry Mo deposits of both arc-related and Climax-type, then any setting with suitable magmatic-hydrothermal architectures that provide optimum conditions for metal deposits could become targets for exploration.

Over the past two decades, over 60 porphyry (-skarn) Mo deposits and occurrences have been found in northeastern (NE) China (Ouyang et al. 2013, 2020, 2021; Chen et al. 2017; Shu et al. 2016, 2021), making NE China the largest Mo ore region on Earth (total Mo resource >12.0 Mt; Shu and Chiaradia 2021). The deposits and occurrences in NE China differ in terms of their tectonic settings, from compressional arc-continent subduction and continent-continent collision to extensional post-subduction, and are all recognizable members of the established porphyry Mo deposits family (Ouyang et al. 2013; Shu et al. 2016; Chen et al. 2017). These features make NE China an ideal location in which to investigate the above-outlined questions regarding the formation of porphyry Mo deposits.

In this contribution, one Climax-type porphyry Mo deposit (i.e., Hashitu; Fig. 1a) and three arc-related porphyry-skarn Mo deposits (i.e., Songbei, Yangjiazhangzi, and Lanjiagou; Figs. 1a–1b) from NE China were selected for study. We present major and trace elements, zircon Hf isotope, and silicate melt inclusion data (providing information about the magmatic volatile and metal budget) for barren and mineralized intrusions of the four deposits. A subset of the data used in this paper has already been published in Ouyang et al. (2020), but the interpretations presented here are new. In combination with our field observations, we aim to: (1) examine the importance of source protolith, magmatic processes, and intensive variables (e.g., magma volatile content, oxygen fugacity, and emplacement depth) in producing porphyry Mo deposits; (2) discuss the results of the present study in comparison with published works on porphyry Mo deposits worldwide; and (3) provide a robust body of evidence to better understand the key factors affecting the formation of porphyry Mo deposits of both arc-related and Climax-type.

Geological background

Geology of the Songbei-Yangjiazhangzi-Lanjiagou ore zone

The Songbei-Yangjiazhangzi-Lanjiagou ore zone is located in the eastern part of the North China Craton (NCC; Fig. 1a), an Archean craton that was extensively thinned during the late Mesozoic by delamination of the lithospheric mantle (Xu et al. 2006). It consists of three large (≥0.1 Mt; Chen et al. 2017) porphyry (-skarn) Mo deposits; Songbei, Yangjiazhangzi, and Lanjiagou. The three Mo deposits are all associated with an Early Jurassic composite intrusive complex, the Yangjiazhangzi pluton (Fig. 1b; Ouyang et al. 2020). The bulk of the Yangjiazhangzi pluton comprises coarse-grained syenogranite, which varies from equigranular to porphyritic, with an outcrop area of ~200 km^2 (Fig. 1b), and was intruded by the fine-grained syenogranite and granite porphyry intrusions (Huang et al. 1994; Wu et al. 2006). Several previous studies proposed that the Early Jurassic magmatism at Songbei-Yangjiazhang-Lanjiagou (subsequently abbreviated as SYL) formed in a continent-continent collisional setting related to the collision between the NCC and the amalgamated terranes of the Central Asian Orogenic Belt (CAOB; e.g., Xiao et al. 2003; Zhang et al. 2014). However, an active continental margin related to the subduction of the Paleo-Pacific plate has also been proposed by other workers (e.g., Chen et al. 2007; Ge et al. 2007; Han et al. 2009; Goldfarb et al. 2021). For these reasons the porphyry (-skarn) deposits in SYL ore zone were classified as arc-related end-members of the established porphyry Mo deposit family (e.g., Zeng et al. 2013; Ouyang et al. 2013, 2020; Shu et al. 2016; Shu and Chiaradia 2021).

Songbei is a skarn Mo deposit and contains an indicated resource of 0.17 Mt Mo at an average grade of 0.10 wt% (Zeng et al. 2013). Intrusive rocks throughout the mining area comprise pre-mineralization fine-grained syenogranite, syn-mineralization granite porphyry, and post-mineralization diabase (Fig. 1c; Zeng et al. 2013; Chu et al. 2017; Ouyang et al. 2020). The granite porphyry, exposed as dikes, intruded along the contact zones between the Permian sandstone and Proterozoic to Paleozoic limestone or into the Proterozoic to Paleozoic limestone, within which most of the Mo mineralization occurs. Molybdenum mineralization in the Songbei deposit is represented by molybdenite-quarzt±pyrite veinlets with sericite and chlorite envelopes in the granite porphyry, or molybdenite-bearing skarn veins, lenses, and mantos (blanketlike body along the bedding plane of the rock) in the limestone (Chu et al. 2017; Ouyang et al. 2020). Laser ablation-inductively coupled plasma-mass spectrometer (LA-ICP-MS) zircon U-Pb dating shows that the intrusion age of the granite porphyry is 184.0 ± 2.0 Ma (1σ, weighted mean $^{206}Pb/^{238}U$ age; Chu et al. 2017), in agreement with the isotope dilution inductively coupled plasma mass spectrometry (ID-ICP-MS) molybdenite Re-Os weighted mean model age of 183.2 ± 3.0 Ma (2σ) within uncertainty (Chu et al. 2017). In the present study, the syn-mineralization rhyolite porphyry phase (previously called granite porphyry) collected from the open pit (Fig. 1c) was chosen for further study. The rhyolite porphyry

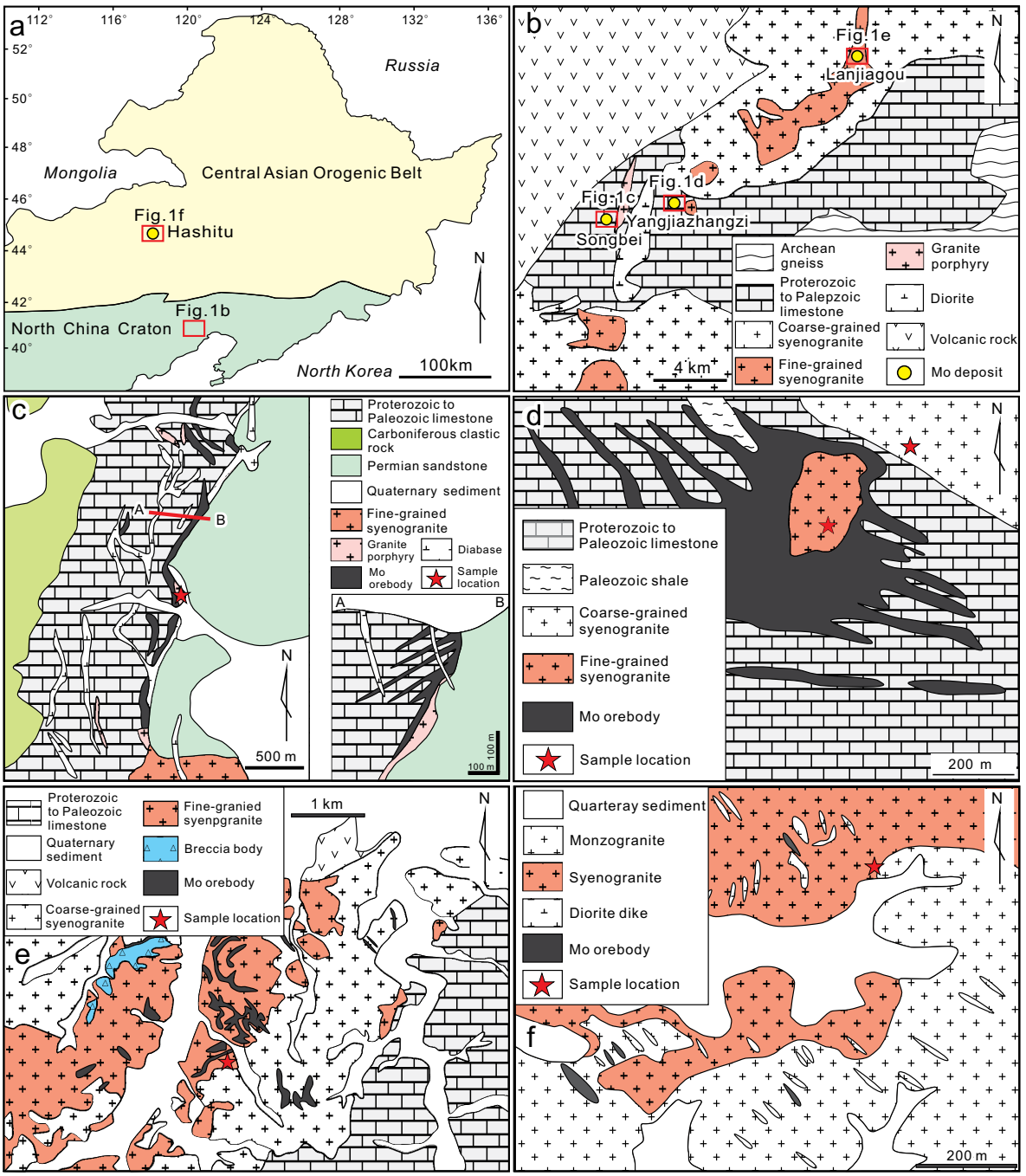

Figure 1. (**a**) Simplified geological map of northeastern China, showing the main tectonic units and deposits investigated in this study. (**b**) Simplified geological map of the area around the Yangjiazhangzi, Lanjiagou, and Songbei deposits (modified from Wu et al. 1990). (**c**) Geological map and cross-section of Songbei (Chu et al. 2017). (**d**) Geological map of Yangjiazhangzi (Han et al. 2009). (**e**) Geological map of Lanjiagou (Han et al. 2009). (**f**) Simplified geological map of Hashitu (Zhai et al. 2018). (Color online.)

(Fig. 2a) contains phenocrysts of quartz, pink alkali feldspar, and biotite, set in an aphanitic groundmass of similar mineralogy; accessory minerals include apatite, titanite, zircon, and magnetite.

The Yangjiazhangzi skarn Mo deposit is located ca. 3.0 km east of the Songbei deposit (Fig. 1b). It contains 0.26 Mt Mo at an average grade of 0.14 wt% (Huang et al. 1989). Intrusive rocks throughout the mining area comprise pre-mineralization coarse-grained syenogranite and syn-mineralization fine-grained syenogranite (Fig. 1d; Ouyang et al. 2020). The coarse-grained syenogranite varied from equigranular to slightly porphyritic and was intruded by the stock-like fine-grained syenogranite (Huang et al. 1994). Zircon U-Pb dating of the coarse-grained

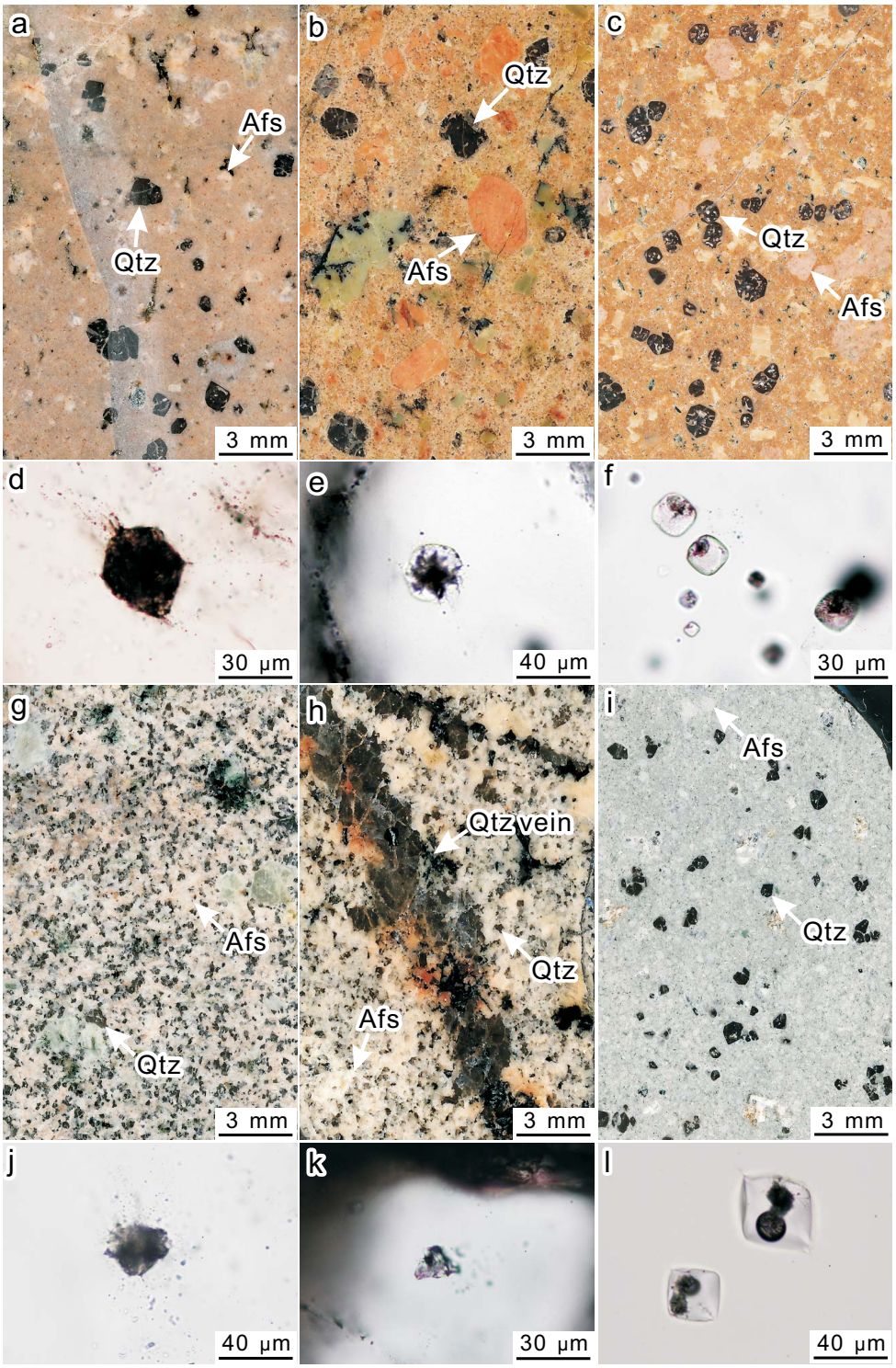

Figure 2. Photographs of polished thick sections and melt inclusions in quartz. (**a**) Songbei syn-mineralization rhyolite porphyry. (**b**) Yangjiazhangzi pre-mineralization granite porphyry. (**c**) Yangjiazhangzi syn-mineralization rhyolite porphyry. (**d**) Finely crystallized melt inclusions in samples from the Songbei deposit. (**e**–**f**) Finely crystallized to glassy melt inclusions from the Yangjiazhangzi syn-mineralization intrusions. (**g**) Lanjiagou fine-grained syenogranite. (**h**) Hashitu pre-mineralization porphyritic monzogranite. (**i**) Hashitu syn-mineralization rhyolite porphyry. (**j**) Decrepitated, finely crystallized melt inclusions from the Lanjiagou fine-grained syenogranite. (**k**) Coarsely crystallized melt inclusions from the Hashitu pre-mineralization intrusion. (**l**) Partly crystallized melt inclusions from the Hashitu syn-mineralization intrusion. Afs = alkali feldspar; Qtz = quartz. (Color online.)

syenogranite yielded a weighted mean $^{206}Pb/^{238}U$ age of 186.1 ± 2.6 Ma (1σ, Cui 2019). The fine-grained syenogranite intrusion is commonly equigranular in texture, but some parts are porphyritic (Ishihara and Shibata 1980). Skarn Mo mineralization occurs mainly in Precambrian carbonate rocks around the fine-grained syenogranite intrusion as massive skarns and skarn veins, with a minor proportion occurring as molybdenite-quarzt±pyrite veinlets hosted in the fine-grained syenogranite intrusion (Fig. 1d; Huang et al. 1994). Zircon U-Pb dating of the fine-grained syenogranite returned a weighted mean $^{206}Pb/^{238}U$ age of 183.7 ± 2.2 Ma (1σ; Cui 2019); in agreement with the molybdenite Re-Os model ages of 187.0 ± 2.0 to 191.0 ± 6.0 Ma (2σ) within uncertainty (Huang et al. 1994). Samples of the pre-mineralization granite porphyry (previously called porphyritic syenogranite; Fig. 2b) and syn-mineralization granitic to rhyolitic porphyry (Fig. 2c) were collected from outcrops and ore heaps (dumps) for the present study. In hand specimen the pre-mineralization granite porphyry contains quartz, pink alkali feldspar, plagioclase and biotite set in a fine-grained groundmass of similar mineralogy. Accessory minerals include apatite, titanite, zircon, and magnetite. The main igneous minerals of the syn-mineralization granitic to rhyolitic porphyry include quartz, pink alkali feldspar, and biotite, with additional minor and trace minerals including zircon, titanite, and magnetite.

The Lanjiagou deposit is located ca. 20 km northwest of the Yangjiazhangzi deposit (Fig. 1b), which has an indicated resource of 0.22 Mt Mo at an average grade of 0.13 wt% (Huang et al. 1989). Mineralization at Lanjiagou is characterized by molybdenite-bearing quartz veins, veinlets, or breccias with sericite and chlorite alterations hosted by a composite intrusive complex, comprising pre-mineralization coarse-grained syenogranite and syn-mineralization fine-grained syenogranite (Fig. 1e; Ouyang et al. 2020). The pre-mineralization coarse-grained syenogranite constituted the bulk of the composite intrusion and was intruded by the stock-like syn-mineralization fine-grained syenogranite. Zircon U-Pb dating of the fine-grained syenogranite gave a weighted mean $^{206}Pb/^{238}U$ age of 185.0 ± 1.8 Ma (1σ; Zheng et al. 2014), which agrees within error with the molybdenite Re-Os weighted mean model age of 183.1 ± 0.8 Ma (2σ; Han et al. 2009). Samples of the syn-mineralization fine-grained syenogranite were chosen for further study. The syn-mineralization fine-grained syenogranite (Fig. 2g) is equigranular and contains quartz, pink alkali feldspar, and biotite. Accessory minerals include zircon, magnetite, apatite, and titanite.

Geology of the Hashitu Mo deposit

The Hashitu deposit is situated in the eastern part of the CAOB (Fig. 1a), a composite accretionary orogen formed by the evolution of the Paleo-Asian ocean during the Paleozoic to Triassic (Windley et al. 2007; Zhang et al. 2019; Liu et al. 2020), and by the evolution of the Paleo-Pacific ocean and Mongolia-Okhotsk ocean during the Early Jurassic to Cretaceous (Wu et al. 2005; Xu et al. 2013). The deposit contains an indicated resource of 0.13 Mt Mo at an average grade of 0.13 wt% (Zhai et al. 2018). Mineralization in the deposit is characterized by molybdenite-bearing quartz±fluorite veins, veinlets, or breccias with sericite and chlorite alteration in the pre-mineralization monzogranite and syn-mineralization syenogranite (Fig. 1f; Online Materials[1] Fig. 1; Zhang et al. 2012; Zhai et al. 2014, 2018; Ouyang et al. 2020), which are the two main lithologies cropping out in the deposit. The pre-mineralization monzogranite varies from coarse equigranular to slightly porphyritic and is exposed in the southern part of the deposit, where it covers an area of ca. 8 km^2 (Fig. 1f). It has a zircon U-Pb weighted mean $^{206}Pb/^{238}U$ age of 147.0 ± 1.0 Ma (1σ; Zhai et al. 2014). The stock-like syn-mineralization syenogranite intruded the monzogranite and crops out mainly in the northern part of the deposit. Zircon U-Pb dating yielded a weighted mean $^{206}Pb/^{238}U$ age of 143.0 ± 2.0 Ma (1σ) for the syenogranite (Zhai et al. 2014). ID-ICP-MS molybdenite Re-Os dating yielded model ages varying from 150.0 ± 2.0 to 144.0 ± 2.0 Ma (2σ) and a weighted mean Re-Os model age of 147.0 ± 1.0 Ma (2σ, n = 9; Zhai et al. 2014). The magmatism and mineralization ages at Hashitu are coeval with the timing of exhumation of metamorphic core complexes, extensive mafic to felsic magmatism, and development of intracontinental rift basins throughout the eastern segment of the CAOB (Meng 2003; Wu et al. 2011). For this reason, the Hashitu porphyry Mo deposit was classified as Climax-type end-member of the established porphyry Mo deposits family (e.g., Zhai et al. 2014; Chen et al. 2017; Ouyang et al. 2020; Shu and Chiaradia 2021). Diamond drilling at Hashitu has revealed the presence of rhyolite porphyry and granite porphyry dikes at depth, and these dikes are also genetically related to the ore-forming hydrothermal event (Online Materials[1] Fig. 1; Zhang et al. 2012; Ouyang et al. 2020). Samples of the pre-mineralization porphyritic monzogranite and monzogranite, together with the syn-mineralization granite porphyry and rhyolite porphyry, all collected from drill cores, were chosen for further study. The main igneous minerals of the pre-mineralization porphyritic monzogranite and monzogranite (Fig. 2h) include quartz, plagioclase, pink alkali feldspar, and biotite, with additional minor and trace zircon, fluorite, titanite, and magnetite (Online Materials[1] Fig. 2). The syn-mineralization granite porphyry and rhyolite porphyry (Fig. 2i) are gray and consist of phenocrysts of quartz, alkali feldspar, and biotite set in fine-grained to aphanitic groundmass of the same mineralogy. Accessory minerals include zircon, fluorite, magnetite, ilmenorutile, monazite, xenotime and molybdenite (the latter occurring primarily as inclusions in quartz phenocrysts; Online Materials[1] Fig. 2; Ouyang et al. 2020).

Methods

Whole-rock major and trace element analysis

Whole-rock major and trace element compositions were analyzed at the Institute of Crust Dynamics, China Earthquake Administration. For major element analysis, powdered samples were fluxed with $Li_2B_4O_7$ at a mass ratio of 1:8 to produce homogeneous glass disks at 1250 °C using a V8C automatic fusion machine. The bulk rock major elements were analyzed on fused glass discs using a Zetium sequential X-ray fluorescence spectrometer. The value of loss on ignition (LOI) was determined at a temperature of 1000 °C. The accuracy and precision of the analytical results were monitored using the GSR-3 and BHVO-2 standards. Analytical errors were better than 2%.

Trace element analysis was conducted using solution inductively coupled plasma mass spectrometry (ICP-MS) on a Thermo-Fisher X Series II. For the digestion procedure, 25 mg of sample powder was precisely weighed and transferred into a screw-top polytetrafluoroethylene beaker. Powders were dissolved in a mixture of concentrated HF-HNO_3 acids (1:5) at 170 °C for 72 h. Once dissolved, solutions were evaporated at 120 °C and twice redissolved using 10.4 mol/L HNO_3. The final solutions were then diluted 1000 times using 2% distilled super-pure HNO_3 for ICP-MS analysis with In, Rh, and Re as internal standards. Standard solutions from American Lab Tech Company were diluted to 1, 10, 50, and 100 μg L^{-1} to produce the calibration curves, which showed linear regression coefficients

≥0.9999. GSR-3 and BHVO-2 standards were run as unknowns to evaluate the accuracy and precision of the analytical results. Analytical errors for most elements were better than 2%.

Zircon Hf isotope analysis

Zircon Hf isotope analysis was carried out using a Nu Plasma II MC-ICP-MS (Nu Instruments) equipped with a 193 nm ArF excimer laser at the Nanjing FocuMS Technology Co. Ltd, China. A circular 50 μm laser spot with a fluence of 6.0 J/cm^2, a repetition rate of 8 Hz, and a duration of 40 s were selected for analysis. Helium was used as the carrier gas to transport the ablated aerosol to the mass spectrometer. Mass fractionation corrections for Hf and Yb isotopic ratios were based on $^{176}Lu/^{175}Lu = 0.02656$ (Blichert-Toft et al. 1997) and $^{176}Yb/^{173}Yb = 0.7876$ (McCulloch et al. 1977), respectively. To monitor the accuracy of this correction, every 5 sample analyses were bracketed by analysis of reference zircons (91500, GJ-1, Mud Tank, Penglai, and Plešovice). During analysis, the standard zircons gave $^{176}Hf/^{177}Hf$ ratios consistent with recommended values (Sláma et al. 2008; Yuan et al. 2008), within analytical error. A decay constant for ^{176}Lu of 1.867×10^{-11} a^{-1} was adopted (Söderlund et al. 2004). Initial $^{176}Hf/^{177}Hf$ ratios, denoted as $\varepsilon_{Hf}(t)$, were calculated relative to the chondritic reservoir with a $^{176}Hf/^{177}Hf$ ratio of 0.282772 and $^{176}Lu/^{177}Hf$ of 0.0332 (Blichert-Toft and Albarède 1997). Single-stage Hf model ages (T_{DM}) were calculated relative to the depleted mantle, which is assumed to have undergone linear isotopic growth from $^{176}Hf/^{177}Hf = 0.279718$ at 4.55 Ga to 0.283250 at the present day with a $^{176}Lu/^{177}Hf$ ratio of 0.0384 (Griffin et al. 2000). Two-stage Hf model ages (T_{2DM}) were calculated assuming a mean $^{176}Lu/^{177}Hf$ value of 0.015 for the average continental crust (Griffin et al. 2002).

Melt inclusion major and trace element analysis

Melt inclusion major and trace element compositions were analyzed in non-homogenized melt inclusions by LA-ICP-MS and in re-homogenized melt inclusions by electron microprobe (EPMA) at the Bayerisches Geoinstitut, Germany. Detailed analytical methods have been described previously by Audétat (2015) and Ouyang et al. (2020).

For major and trace element analysis of non-homogenized melt inclusions, selected inclusions from doubly polished thin sections were analyzed with a 193 nm ArF Excimer laser ablation system coupled to a PerkinElmer Elan DRC-e quadrupole ICP-MS. The laser was operated at 5–10 Hz with an energy density of 3–10 J cm^{-2}. The diameter of the laser beam was chosen to ensure ablation of the entire melt inclusion while keeping the amount of ablated host mineral (i.e., quartz) to a minimum. NIST SRM 610 was used as the external standard and was analyzed twice at the beginning and end of each block of up to 20 analyses. A well-characterized in-house obsidian standard was analyzed in each session as an unknown to check accuracy. Before each melt inclusion analysis, the quartz host was analyzed nearby using a 40 μm circular spot to obtain a signal that could be used for Ti-in-quartz (TitaniQ) thermobarometry (Huang and Audétat 2012). Internal standardization of the melt inclusions was based on SiO_2 vs. Al_2O_3 trends defined by corresponding whole-rock data shown in Online Materials[1] Table OM1. Uncertainties associated with the analyses for most of the elements are estimated at 5 to 7%.

To estimate the volatile contents (S, F, Cl, and H_2O) of magmas, melt inclusions in quartz phenocrysts were re-homogenized at conditions of 1.5 to 2.0 kbar and 780 °C. The re-homogenized melt inclusions were then polished to the surface and subsequently analyzed using a JEOL JXA-8200 microprobe, using 15 kV, 20 nA beam that was defocused to 10 μm. Standardization was performed on albite (Na, Si), orthoclase (K), spinel (Al), $MnTiO_3$ (Mn, Ti), metallic Fe, enstatite (Mg), wollastonite (Ca), fluorite (F), vanadinite (Cl), and barite (S). A topaz crystal containing 20.5 ± 0.5 wt% F was measured as an unknown and returned expected F values of 20.1 ± 0.2 wt%. Estimated H_2O contents of the re-homogenized melt inclusions were obtained by taking the difference of the measured major element analytical total to 100 wt% and taking into account O=F substitution (i.e., H_2O contents equal 100 wt% minus the measured major element analytical total and O=F substitution value; Devine et al. 1995). Due to alkali migration or Na loss during EPMA analysis (e.g., Devine et al. 1995; Donovan and Vicenzi 2008), the estimated H_2O contents are associated with an error of at least ±1 wt%.

Results

Major and trace elements

Whole-rock major and trace element compositions for the pre- and syn-mineralization intrusive samples from the arc-related SYL ore zone and Climax-type Hashitu deposit are listed in Online Materials[1] Table OM1 and shown in Figure 3. All the syn-mineralization intrusive samples are quite evolved, with SiO_2 contents between 71.79 and 77.06 wt% and total alkali content (Na_2O+K_2O) of 6.74 to 9.19 wt% (Fig. 3a). On the SiO_2 vs. K_2O diagram, they show high-K calc-alkaline to shoshonite affinities (Fig. 3b). When plotted in primitive mantle-normalized trace element diagrams (Figs. 3c and 3e), all samples display similar patterns characterized by enrichments in Rb, Th, U, and Pb, and depletions in Ba, Nb, Sr, and Eu. On the chondrite-normalized rare earth element (REE) diagrams (Figs. 3d and 3f), all samples are enriched in light rare earth elements (LREE) with respect to heavy rare earth elements (HREE; $La_N/Yb_N = 2.7–33.1$) and show little to moderate fractionation between the middle REE (MREEs) and HREE ($Dy_N/Yb_N = 0.4–1.3$) with apparent negative Eu anomalies (Eu* = 0.02–0.69).

Despite some compositional overlap, variations in the trace element systematics of the syn-mineralization intrusions from the Hashitu deposit and SYL ore zone can be discerned. The syn-mineralization intrusions from the Hashitu deposit generally have low concentrations of Sr (11–52 ppm) and Ba (14–87 ppm) and high concentrations of Y (25–63 ppm; Online Materials[1] Table OM1). Their chondrite-normalized REE patterns are generally flat ($La_N/Yb_N = 3.2–6.9$) and exhibit strong negative Eu anomalies (Eu/Eu* = 0.02–0.10; Fig. 3d). In contrast, the syn-mineralization intrusions from the SYL ore zone are relatively enriched in Sr (60–179 ppm) and Ba (124–591 ppm), and depleted in Y (7.8–29.0 ppm; Online Materials[1] Table OM1). Their chondrite-normalized REE patterns show apparent LREE enrichment ($La_N/Yb_N = 2.7–33.1$) and moderately negative Eu anomalies (Eu/Eu* = 0.4–0.7).

In addition, except for crosscutting relationships and petrographic differences (Figs. 1–2; Ouyang et al. 2020), it is difficult to distinguish the pre- and syn-mineralization intrusions in the individual deposits on the basis of their major and trace element geochemistry (Fig. 3). This observation may reflect a common magma source and similar extent of fractionation of the pre- and syn-mineralization intrusions in the individual deposits investigated in the present study.

Zircon Hf isotopes

Zircon Hf isotopic compositions for the pre- and syn-mineralization intrusions from the SYL ore zone and Hashitu deposit are reported in Online Materials[1] Table OM2 and shown in Figure 4. Zircons from the Yangjiazhangzi syn-mineralization intrusion are characterized by enriched initial $^{176}Hf/^{177}Hf$ values that vary between 0.282302 and 0.282456. Their corresponding initial $\varepsilon_{Hf}(t)$ values are restricted to –12.6 to –7.1 (–7.6 on average, n = 16), which are similar to those of the Yangjiazhangzi pre-mineralization intrusion of –12.1 to –7.5 (–9.2 on average, n = 14). The 19 analyzed zircons from the Lanjiagou syn-mineralization intrusion yield a range of initial $\varepsilon_{Hf}(t)$ values of –11.9 to –7.8 (–9.8 on average), which is comparable to the pre- and syn-mineralization intrusions from the Yangjiazhangzi deposit. Zircons from the Songbei syn-mineralizations intrusion show relatively less enriched initial $\varepsilon_{Hf}(t)$ values of –10.7 to –4.9 (–7.6 on average, n = 20).

Initial $^{176}Hf/^{177}Hf$ values of the zircons from the Hashitu syn-mineralization vary between 0.282772 and 0.282824 (Online Materials[1] Table OM2). Corresponding initial $\varepsilon_{Hf}(t)$ values rang-

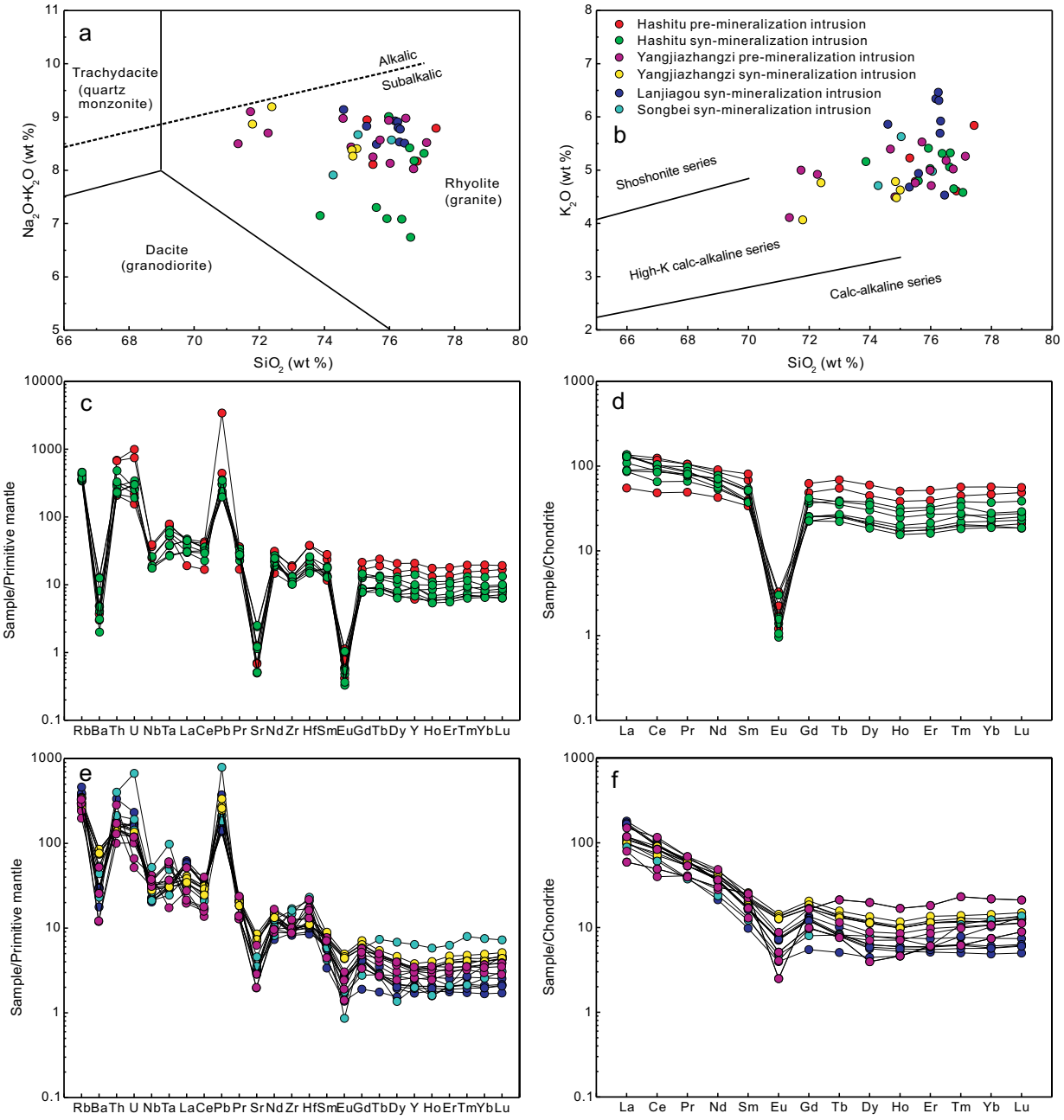

Figure 3. (**a**) Total alkalis (Na_2O+K_2O) vs. SiO_2 diagram (TAS; Le Bas et al. 1986) and (**b**) K_2O vs. SiO_2 diagram showing the geochemical classification of the whole-rock samples from the deposits investigated in this study. The dashed line separating alkaline series from subalkaline series is from Irvine and Baragar (1971). (**c**–**d**) Primitive mantle-normalized trace element diagram and chondrite-normalized REE patterns for samples from the Hashitu deposit. (**e**–**f**) Primitive mantle-normalized trace element diagram and chondrite-normalized REE patterns for samples from the Songbei-Yangjiazhangzi-Lanjiagou ore zone; normalized values from Sun and McDonough (1989). (Color online.)

ing from 3.1 to 5.0 (4.1 on average, n = 19). Zircons from the Hashitu pre-mineralizations intrusion yield initial $\varepsilon_{Hf}(t)$ values [$\varepsilon_{Hf}(t)$ = 2.1–4.4, 2.8 on average] similar to those of the Hashitu syn-mineralization intrusion but are in marked contrast to the initial zircon $\varepsilon_{Hf}(t)$ values of the pre- and syn-mineralization intrusions from the SYL ore zone (Fig. 4).

Melt inclusion compositions

The Songbei-Yangjiazhangzi-Lanjiagou ore zone. LA-ICP-MS and EPMA data for melt inclusions from the SYL ore zone and Hashitu deposit are provided in Online Materials[1] Tables OM3 and OM4. Melt inclusions from the Yangjiazhangzi pre-mineralization intrusion are highly evolved

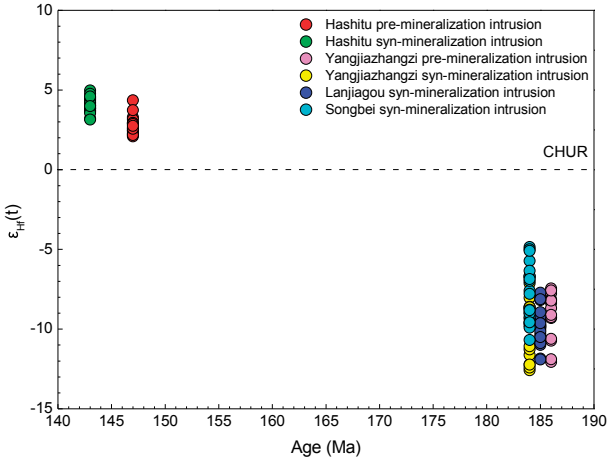

Figure 4. Initial zircon Hf isotopic compositions of the pre- and syn-mineralization intrusions at their crystallization ages from the Songbei-Yangjiazhangzi-Lanjiagou ore zone and Hashitu deposit. CHUR = chondritic uniform reservoir mantle. (Color online.)

(SiO_2 = ~80 wt%), with 346 to 438 ppm Rb, 5 to 11 ppm Cs, and 4 to 6 ppm Mo (Online Materials[1] Table OM3). No data on the volatile contents of the melt inclusions from the Yangjiazhangzi pre-mineralization intrusion were obtained in this study due to their relatively poorly preserved condition. Melt inclusions from the Yangjiazhangzi syn-mineralization intrusion are finely crystallized to glassy (Figs. 2e and 2f). They are slightly less evolved than those of the pre-mineralization intrusion (Rb = 171–265 ppm; Cs = 4–6 ppm), except one that contains 209 ppm Rb and 24 ppm Cs. Molybdenum concentrations in the melt inclusions show a narrow range of 2 to 4 ppm. The melt inclusions contain ≤0.05 wt% Cl and variable H_2O (4.6 to 7.4 wt%), whereas F contents were below the detection limit (0.15 wt%; Online Materials[1] Table OM4).

Melt inclusions from the Lanjiagou syn-mineralization intrusion are finely crystallized (Fig. 2j). They are comparable in composition with the melt inclusions from the Yangjiazhangzi pre- and syn-mineralization intrusions, which are also highly evolved (78–79 wt% SiO_2) with 222 to 341 ppm Rb, 2 to 8 ppm Cs, and 4 to 5 ppm Mo. No data on volatile contents were obtained for the melt inclusions from the Lanjiagou syn-mineralization intrusion due to scarcity and the poorly preserved nature of the inclusions.

Melt inclusions from the Songbei syn-mineralization intrusion are finely crystallized (Fig. 2d). They are highly evolved (SiO_2 = ~79 wt%) and typically contain 139 to 242 ppm Rb and 2 to 9 ppm Cs, except three that contain considerable Rb (305–1269 ppm) and Cs (20–88 ppm). However, Mo concentrations in the melt inclusions are relatively constant at 1 to 5 ppm. No volatile content data are presented for the melt inclusions from the Songbei syn-mineralization intrusion because the inclusions are partially decrepitated and thus were not considered for re-homogenization.

The Hashitu deposit. Melt inclusions from the Hashitu pre-mineralization intrusion are coarsely crystallized (Fig. 2k). They are rhyolitic in composition (SiO_2 = ~80 wt%) with 301 to 646 ppm Rb and 5 to 48 ppm Cs (Online Materials[1] Table OM3). Molybdenum concentrations in the melt inclusions show a narrow range of 1 to 5 ppm. Melt inclusions from the Hashitu syn-mineralization intrusions are partly crystallized (Fig. 2i) and contain 198 to 731 ppm Rb, 8 to 53 ppm Cs, and 1 to 7 ppm Mo, comparable with those from the Hashitu pre-mineralization intrusion. They contain 4.4 to 7.8 wt% H_2O, ≤0.4 wt% F, and 0.03 to 0.09 wt% Cl (Online Materials[1] Table OM4).

Discussion

Producing a porphyry Mo deposit clearly requires a series of favorable geological conditions and processes, including partial melting of magma source regions in the lower crust, the bulk composition of the magma, the metal and volatile content of the magma, the oxidation state and crystallization conditions, and the mechanisms of magma emplacement and volatile exsolution in the upper crust (Richards 2011a and references therein). Moreover, there are two major classes of porphyry Mo deposits (i.e., arc-related and Climax-type; Carten et al. 1993; Ludington and Plumlee 2009; Taylor et al. 2012), which show contrasting tectonic settings and geochemistry of associated intrusions. Such features raise an additional set of petrogenetic and metallogenic questions relating to the formation of porphyry Mo deposits. In the following sections, the various contributing factors mentioned above are critically assessed based on the data presented in the present and former studies.

Influence of magma source

As shown in Figure 4, zircon Hf isotopic compositions of the syn-mineralization intrusions from the arc-related SYL deposits are comparable, with most values centered around –12.0 to –8.0. These values indicate that the parental magma of the syn-mineralization intrusions from the SYL ore zone was most likely produced by partial melting of ancient lower crust (Jiang et al. 2009), or through the interaction of enriched-mantle derived melts with ancient crustal rocks and/or melts (Chen et al. 2007). By contrast, the initial Hf isotopic compositions of the zircons from the Climax-type Hashitu syn-mineralization intrusions are more radiogenic [$\varepsilon_{Hf}(t)$ = 3.1–5.0; Fig. 4], implying that their parental magmas were most likely produced by partial melting of the juvenile lower crust, probably initiated by upper mantle basaltic melts interacting with crustal rocks and/or melts (Wu et al. 2002, 2003). Such contrasting zircon Hf isotopic compositions of the syn-mineralization intrusions between the SYL ore zone and the Hashitu deposit may relate to the two fundamentally different orogenic systems from which the parental magmas originated. The SYL ore zone is located in a reactivated Archean craton (Fig. 1a). The lower crust beneath the craton mainly consists of ancient crustal material (Xu et al. 2006). In contrast, the Hashitu deposit is situated in the eastern part of the CAOB (Fig. 1a), which is a composite accretionary orogen formed by the evolution of the Paleo-Asian, Paleo-Pacific, and Mongolia-Okhotsk oceans during the Phanerozoic (Wu et al. 2005; Windley et al. 2007; Xu et al. 2013). The lower crust of the CAOB, therefore, comprises juvenile material, which generates a distinct radiogenic hafnium signature when remelted (Wu et al. 2002, 2003; Windley et al. 2007).

In fact, similar disparate isotope compositions of the syn-

mineralization intrusions were not only observed among arc-related and Climax-type porphyry Mo deposits, but also in the same class of porphyry Mo deposits. For example, previous studies on the world-class Climax-type deposits (e.g., Henderson and Climax) in the middle Rocky Mountains, western North America, showed that the parental magmas of the causative intrusions in these deposits were derived from enriched lithospheric mantle or ancient crust (Keith et al. 1993; Pettke et al. 2010), contrasting with the syn-mineralization intrusions from the Climax-type Hashitu deposit. Neodymium isotopic compositions of the syn-mineralization intrusions from the arc-related Endako porphyry Mo deposit indicate that the parental magmas of the causative intrusions in this deposit were mainly formed by partial melting of juvenile material (Whalen et al. 2001), which is in marked contrast to the syn-mineralization intrusions from the arc-related SYL deposits.

The above discussion indicates that unique magma sources may not be required for the formation of porphyry (-skarn) Mo deposits of both arc-related and Climax-type. This conclusion is further supported by the zircon Hf isotopic compositions of the pre-mineralization intrusions from the Songbei-Yangjiazhangzi-Lanjiagou ore zone and Hashitu deposit, which are comparable to those of the syn-mineralization intrusions in the individual cases (Fig. 4). Consequently, in addition to the nature of the magma source, other factors may be more critical for the formation of both arc-related and Climax-type porphyry Mo deposits.

Influence of the bulk composition of ore-forming magmas

Whole-rock major and trace element data show that the geochemistry of associated intrusions of the two classes of porphyry Mo deposits investigated in the present study exhibit certain characteristics that make each class unique. The syn-mineralization intrusions from the Climax Hashitu deposit are depleted in TiO_2 (0.07 wt% on average), Sr (11–52 ppm) and Ba (14–89 ppm), and enriched in Rb (280 ppm), Nb (15 ppm) and Y (25–94 ppm). They generally exhibit flat chondrite-normalized REE patterns with strong negative Eu anomalies (Fig. 3d) indicating extensive fractional crystallization of a plagioclase-rich assemblage (Whalen et al. 1987; Wu et al. 2017). By contrast, the syn-mineralization intrusions from the arc-related porphyry (-skarn) Mo deposits SYL are relatively enriched in TiO_2 (0.16 wt% on average), Sr (42–179 ppm) and Ba (84–591 ppm), and depleted in Y (7.8–29.0 ppm). Their chondrite-normalized REE patterns are characterized by apparent LREE enrichment and moderate negative Eu anomalies (Fig. 3f), which most likely reflects the predominance of plagioclase-amphibole in the fractionating mineral assemblage or in the restite (Romick et al. 1992; Richards 2011b). The association of Climax-type and arc-related porphyry (-skarn) Mo deposits with distinct bulk magma compositions (as described above) could suggest some sort of petrogenetic control on the formation of porphyry Mo deposits, which has been mainly ascribed to differences in tectonic setting and thermal regime (e.g., Carten et al. 1993; Ludington and Plumlee 2009; Richards 2011a; Taylor et al. 2012). However, compared to intrusions associated with typical Climax-type and arc-related porphyry Mo deposits (Carten et al. 1993; Ludington and Plumlee 2009; Taylor et al. 2012), the syn-mineralization intrusions from the four deposits investigated here exhibit some hybrid characteristics, with Hashitu more closely resembling the former, and SYL the latter. This may suggest that intrusions associated with a certain class of porphyry Mo deposit could show a relatively broad compositional variation. This inference is consistent with the identified geochemical features of the intrusions associated with arc-related porphyry Mo deposits that exhibit a wide variation in SiO_2 contents ranging from 65.0 to 77.0 wt% (Taylor et al. 2012).

The relatively broad compositional variation shown by intrusions associated with a certain class of porphyry Mo deposit can be caused by a variety of mechanisms, including heterogeneous protolith sources, anatectic style and degree of fractional crystallization (Richards 2011a and references therein), and the exact nature for the specific cases investigated in the present study is beyond the scope of this contribution. Meanwhile, it suggests that the bulk composition of ore-forming magmas, which is in turn controlled by other factors, such as tectonic setting, composition of source rocks, degree of partial melting, and the extent of fractionation, is not a critical control on the formation of porphyry Mo deposits of both arc-related and Climax-type. As shown in Figure 3, the bulk compositions of the pre- and syn-mineralization intrusions in the individual deposits of both arc-related and Climax-type are overall similar, further implying other factors are more important for the formation of porphyry Mo deposits.

Molybdenum content of the ore-forming magma

LA-ICP-MS data show that melt inclusions from the syn-mineralization intrusions of the three arc-related Mo deposits in the SYL ore zone are all poor in Mo (ranging from 1 to 5 ppm Mo with an average of 3 ppm) and similar to those of the Climax-type Hashitu deposit of 1 to 7 ppm (Online Materials[1] Table OM3; Fig. 5b). The Mo-poor composition of melt inclusions could result from molybdenite saturation (e.g., Audétat et al. 2011), Mo partitioning into Ti-bearing minerals (Cerny et al. 2005 and references therein), or that Mo was transported into the fluid phase prior to melt inclusion growth (e.g., Audétat 2010). Ouyang et al. (2020) observed magmatic molybdenite inclusions in quartz phenocrysts of the Hashitu syn-mineralization intrusions (Online Materials[1] Fig. 2c). As shown in Figures 5a–5b, the Mo contents of the melt inclusions in this deposit generally increase with an increasing degree of melt fractionation. This may suggest that the magmatic molybdenite inclusions in the Hashitu deposit are too sparse to account for the Mo-poor composition of the analyzed melt inclusions. Moreover, in this study, non-magmatic molybdenite inclusions were observed in the syn-mineralization intrusions of the SYL ore zone. These two observations generally preclude a link between the Mo-poor composition of the analyzed melt inclusions and molybdenite saturation. Under reduced conditions, wherein the dominant speciation of Mo is Mo^{4+}, Mo tends to partition into Ti-bearing minerals (e.g., ilmenite, titanite, and biotite), resulting in Mo-poor magmas, as the ionic radius of Mo^{4+} is nearly identical to Ti^{4+} (Cerny et al. 2005 and references therein). Our petrographic observations show that magnetite and titanite are the common accessory minerals in the syn-mineralization intrusions of the SYL ore zone and Hashitu deposit, indicating the relatively oxidized nature of the syn-mineralization intrusions in both cases

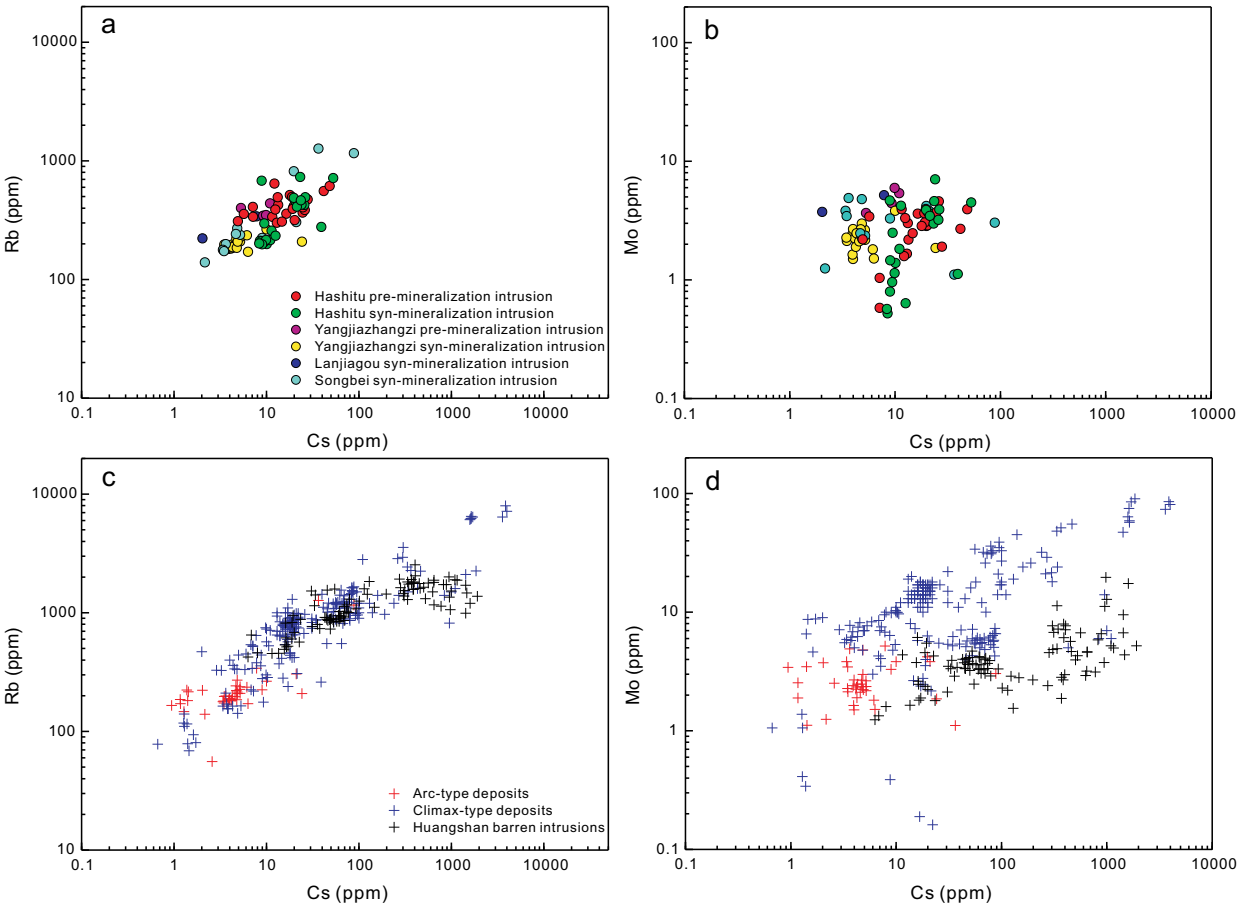

Figure 5. Cs concentrations vs. (**a**) Rb concentrations and (**b**) Mo concentrations in melt inclusions analyzed in the present study. The Cs, Rb, and Mo concentrations (**c**–**d**) in melt inclusions analyzed from Climax-type porphyry Mo deposits (Audétat 2015; Audétat and Li 2017; Zhang and Audétat 2017), arc-related porphyry Mo deposits (Lerchbaumer and Audétat 2013; Ouyang et al. 2021) and Huangshan barren granites (Zhang and Audétat 2018) are shown for comparison. (Color online.)

(e.g., Dilles 1987). It follows that the Mo-poor composition of the melt inclusions investigated in this study cannot be solely ascribed to the partitioning of Mo into Ti-bearing minerals prior to melt inclusion growth.

As shown in Figure 5, the Mo contents of the melt inclusions in the individual deposits investigated in this study generally increase with increasing degree of melt fractionation, as indicated by increasing Rb and Cs concentrations. This feature generally precludes the possibility that Mo is partitioned into magmatic molybdenite, Ti-bearing minerals, or a fluid phase prior to the growth of melt inclusions. In fact, the evolutionary trends of Rb, Cs, and Mo (Figs. 5a–5b) generally overlap with the trends shown by known arc-related and Climax-type deposits (Figs. 5c–5d). This indicates that the melt from which the inclusions formed was, in fact, Mo poor rather than undergoing Mo loss prior to inclusion entrapment. The Mo contents of the syn-mineralization inclusions of the two class of porphyry Mo deposits investigated in this study (2.7 ppm on average; Online Materials[1] Table OM3) are generally higher than the less evolved (SiO_2 < 70 wt%) medium to high-K calc-alkaline granitoids of 1 to 1.5 ppm (Cerny et al. 2005 and references therein), but are consistent with the Mo concentrations of mineralization granitoids (3 to 4 ppm) associated with both typical arc-related and Climax-type deposits (Lowenstern 1994; Audétat 2015; Zhang and Audétat 2017; Ouyang et al. 2021). These results indicate that high-Mo concentrations may not be necessary for the formation of the porphyry Mo deposits of both arc-related and Climax-type, although anomalously Mo rich sources will undoubtedly increase the probability of mineralization. This conclusion is further supported by two observations: (1) no systematic difference in Mo contents between the pre- and syn-mineralization intrusions is evident within each deposit investigated in this study (Fig. 5b), and (2) the melt inclusions investigated in this study contain comparable Mo contents to those of barren intrusions (e.g., Zhang and Audétat 2018).

Effect of magma F and Cl contents

EPMA analysis of the re-homogenized melt inclusions show that melt inclusions from the Climax-type Hashitu syn-mineralization intrusions contain ≤0.4 wt% F, which is in marked contrast to those of the syn-mineralization intrusions from the arc-related SYL ore zone, with F contents below the EPMA detection limit

of 0.15 wt% (Fig. 6a). The relatively F-rich feature of the Hashitu syn-mineralization intrusions is consistent with the occurrence of magmatic fluorite in the intrusions (Online Materials[1] Fig. 2a) and appreciable hydrothermal fluorite in the deposit (Zhai et al. 2018). It also consistent with the observation that porphyry Mo deposits formed in within-plate settings (Climax-type) generally contain more F than their arc-related counterparts (e.g., Carten et al. 1993; Ludington and Plumlee 2009; Zhang and Audétat 2017). However, compared to the two typical Climax-type deposits of Climax and Urad-Henderson, which contain up to 3.9 wt% F (Audétat 2015; Zhang and Audétat 2017), the Hashitu system is still F-poor.

Fluorine is known to extend magma fractionation by reducing minimum-melt temperature and melt viscosity (Dingwell et al. 1985), and thus enhances Mo concentration processes and mineralization potential (Carten et al. 1993). Indeed, as shown in Figures 5c–5d, the most highly fractionated melts (10 times more fractionated than the melts investigated in this study), which have distinctly higher Mo contents (up to 100 ppm), are from the two highly F-enriched Climax-type deposits of Climax (3.1–3.9 wt%; Audétat 2015) and Urad-Henderson

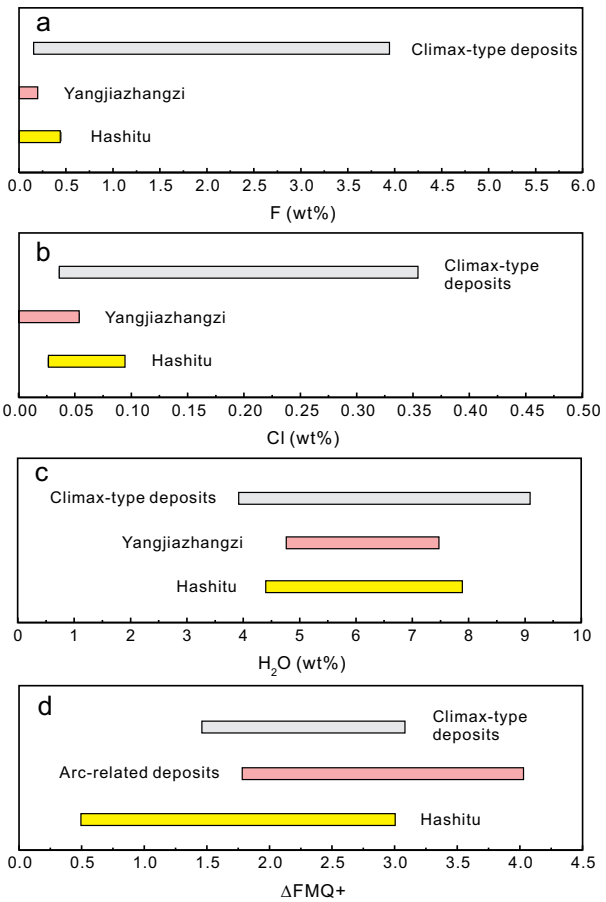

Figure 6. (**a**) F, (**b**) Cl, (**c**) H_2O contents, and (**d**) oxygen fugacities of the ore-forming magmas relating to the deposits investigated in this study and the arc-related and Climax-type Mo deposits. Data sourced from Audétat (2015), Audétat and Li (2017), Zhang and Audétat (2017), Shu et al. (2019), and Xing et al. (2021). (Color online.)

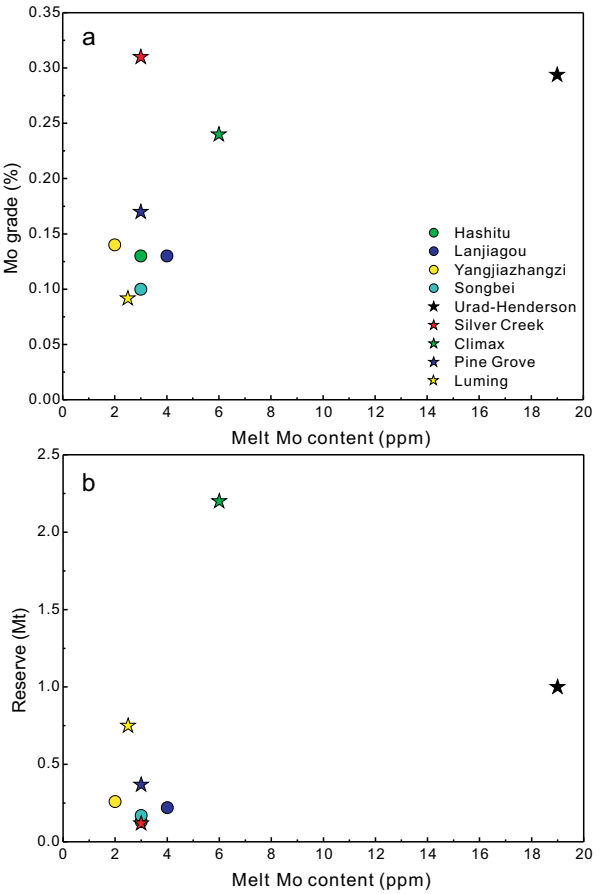

Figure 7. Melt Mo content vs. (**a**) grade and (**b**) reserve for deposits in this study and the arc-related and Climax-type deposits. Data sourced from Carten et al. (1993), Audétat (2015), Audétat and Li (2017), Zhang and Audétat (2017), and Ouyang et al. (2021). (Color online.)

(0.5–1.0 wt%; Zhang and Audétat 2017). Correspondingly, the Mo grades and metal endowments of these deposits are generally higher than other F-poor systems (Fig. 7a). However, this trend is not so apparent in the present and selected existing case studies. For example, compared to melt inclusions from the relatively F-enriched Hashitu (≤0.4 wt% F; this study), Pine Grove (0.2–0.9 wt% F; Lowenstern 1994; Zhang and Audétat 2017) and Silver Creek (0.25–0.32 wt% F; Zhang and Audétat 2017) systems, those from the F-poor SYL systems (<0.15 wt% F; this study) are similar evolved with comparable Mo contents and/or ore grades and reserves (Figs. 5 and 7). This implies that magma F content may not be a prerequisite for the formation of porphyry Mo deposits, although elevated F can indeed extend fractionation and thus enhance the melt Mo concentration and ore grade or reserve.

As shown in Figures 6a–6b, there is a positive correction between magma F and Cl contents. The high-Cl content in F-rich magmas may be related to the fact that F can increase the solubility of Cl in melts (Webster 1997). However, regardless of the Cl content, all magmas studied here produced economic Mo mineralization. This suggests that a high-magma Cl content is also not a requisite to produce economic porphyry Mo mineralization.

This conclusion is permissively consistent with experimental results that demonstrate that, in porphyry Mo systems, Mo is dominantly transported as a hydroxyl complex and that high-Cl concentrations may inhibit the transport of Mo by destabilizing the hydroxyl complex (Keppler and Wyllie 1991).

Influence of magma emplacement depth

In this study, titanium-in-quartz (TitaniQ) thermobarometry of Huang and Audétat (2012) was used to estimate the crystallization pressures (i.e., magma emplacement depths) at which the magmas were emplaced based on melt inclusion LA-ICP-MS data (Online Materials[1] Table OM3). The calculated crystallization pressures for the syn-mineralization intrusions from the arc-related SYL deposits fall within the range of 1.3 to 3.7 kbar, which is comparable with the results of the syn-mineralization intrusions from the Climax-type Hashitu deposit of 0.7 to 2.3 kbar. Taken together, the calculated crystallization pressures for the syn-mineralization intrusions from the SYL ore zone and Hashitu deposit are mostly fall within the range of 1.0 to 2.5 kbar (Fig. 8), corresponding to emplacement depths of 3.3 to 8.3 km. This range of values is similar to those reported for other porphyry Mo systems of both arc-related and Climax-type of 1.5 to 6.0 km (e.g., White et al. 1981; Seedorff et al. 2005; Audétat and Li 2017), and all indicate a relatively shallow emplacement depth for the causative intrusions, which is consistent with the porphyritic textures of the syn-mineralization intrusions (Fig. 2) and the brittle nature of the molybdenite-bearing stockwork veining in the investigated deposits (Ouyang et al. 2020). The reason for the shallow emplacement depth of syn-mineralization intrusions in porphyry systems may lie in the behavior of H_2O, as water solubility in granite melts is strongly related to pressure, rather than being melt composition dependent, with solubility decreasing markedly at pressures below 2.0 kbar (Johannes and Holtz 1996; Burnham 1997). The above evidence suggests that magma emplacement depth most likely plays a fundamental role in the development of porphyry Mo mineralization of both arc-related and Climax-type deposits. As shown in Figure 8, however, no variation in magma emplacement depth is observed between the syn- and pre-mineralization intrusions in the individual deposits investigated here, implying additional factors must also be important.

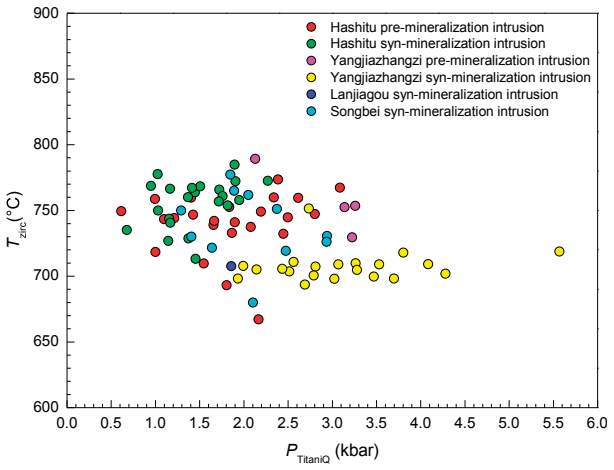

Figure 8. Relationship between entrapment pressures (P) and zircon saturation temperatures (T) of the melt inclusions from the pre- and syn-mineralization intrusions of the Songbei-Yangjiazhangzi-Lanjiagou ore zone and the Hashitu deposit. (Color online.)

Influence of magma water content

Based on estimated crystallization temperatures and pressures of melt inclusions from the Climax-type Hashitu and arc-related Yangjiazhangzi deposits (Online Materials[1] Table OM3), and the water solubility models of Johannes and Holtz (1996) and Holtz et al. (2001), the saturated water contents of ore-forming magmas at Hashitu and Yangjiazhangzi are estimated at 4.2 to 6.2 wt% and 5.1 to 8.6 wt%, respectively. These values are almost identical to those estimated based on melt inclusion EPMA data of 4.4 to 7.8 wt% for Hashitu and 4.6 to 7.4 wt% for Yangjiazhangzi (Online Materials[1] Table OM4), according to the method of Devine et al. (1995). This indicates that the ore-forming magmas at Hashitu and the SYL ore zone were all water-saturated at their emplacement depths. Similar water-saturated ore-forming magmas have also been observed in many other porphyry Mo systems of both arc-related and Climax-type. For example, melt inclusion data show that the ore-forming magmas of the Climax and Urad-Hederson porphyry Mo deposits contain 4.0 to 9.0 wt% H_2O with crystallization pressures of 4.0 to 1.0 kbar (Fig. 6c; Audétat 2015; Zhang and Audétat 2017), indicating water-saturated conditions. Does this mean that some intrusions are barren because their magmas are water-undersaturated at their emplacement depths and hence cannot exsolve sufficient volumes of metal-bearing fluids for mineralization? In this study, the water contents of the pre-mineralization intrusions at their emplacement depths could not be estimated directly due to the poor preservation of melt inclusions. However, we consider that the pre-mineralization intrusions were most likely water-saturated, along with their corresponding syn-mineralization intrusions, as the estimated crystallization pressures, zircon Hf isotopic compositions, and the bulk compositions of the pre- and syn-mineralization intrusions in the individual deposits are comparable. Hence, it appears that, in addition to melt water content, additional factors may also be critical for the formation of porphyry Mo deposits.

Influence of magma oxygen fugacity

Under oxidizing conditions, Mo partitions in favor of the melt over Ti-bearing minerals and thus can enhance the availability of Mo for partitioning into the aqueous phase (Candela and Bouton 1990; Ballard et al. 2002). Hence, oxygen fugacity (f_{O_2}) is an important factor affecting the mineralization potential of porphyry Mo systems (e.g., Cerny et al. 2005; Shu et al. 2019). In this study, due to the rare occurrence of magmatic molybdenite in quartz phenocrysts, only the f_{O_2} of the syn-mineralization granite porphyry from the Climax-type Hashitu deposit was obtained. Based on zircon saturation temperatures of 761 to 785 °C and melt Mo concentrations of 2.5 to 7.0 ppm (Online Materials[1] Table OM3), using the molybdenite solubility model of Audétat et al. (2011), the calculated magma oxygen fugacity for the syn-mineralization intrusions from the Hashitu deposit range from ΔFMQ+0.5 to ΔFMQ+3.0 (ΔFMQ+1.0 on average; Fig. 6d). These values broadly overlap with those constrained for Climax-

type deposits of ΔFMQ = 1.5 to 3.3 (Audétat 2015; Audétat and Li 2017; Zhang and Audétat 2017 and references therein) and for arc-related deposits of ΔFMQ = 1.8 to 4.1 (Shu et al. 2019; Xing et al. 2021), all indicative of oxidized conditions. Accordingly, available evidence suggests that oxidized magmas may play a fundamental role in the formation of porphyry Mo deposits of both arc-related and Climax-type.

Whole-rock major and trace elements and zircon Hf isotope data show that the pre- and syn-mineralization intrusions in the individual deposits investigated in this study have a common magma source and have experienced a similar petrogenetic evolution (Figs. 3–4). Moreover, petrographic observations show that the pre- and syn-mineralization intrusions in the individual deposits are both characterized by the presence of primary titanite and magnetite, and an absence of ilmenite. Together, this evidence indicates that the pre-mineralization intrusions are most likely oxidized as well as their corresponding syn-mineralization intrusions. As not all of them host Mo mineralization, factors other than magma oxygen fugacity likely control the actual ore-forming event in porphyry Mo systems.

Key processes for the formation of porphyry Mo deposits

The evidence presented in the previous sections suggests that magma emplacement depth, water content, and oxygen fugacity play fundamental roles in the genesis of porphyry Mo deposits of both arc-related and Climax-type. However, as not all oxidized, water-saturated magmas emplaced at the favorable depths (i.e., 1.5–6.0 km palaeodepth; Seedorff et al. 2005) develop fertile, magmatic-hydrothermal Mo systems; other factors may therefore be more critical in facilitating the actual ore-forming event in porphyry Mo systems.

The Mo-poor characteristics of many ore-forming magmas, as shown in the present and previous studies, imply that substantial volumes of magma and fluids are required to provide the Mo present in the deposits. For example, assuming the ore-forming magmas have a density of 2.4 g/cm^3 (Fountain and Christensen 1989), a Mo concentration of 2 ppm, and 100% extraction efficiency of Mo from the magma, to account for the 0.26 Mt of Mo present in the Yangjiazhangzi deposit (Huang et al. 1989), at least 26 km^3 of magma is necessary. Meanwhile, at least 2.8 km^3 of intermediate-density fluids are needed, assuming the fluid contains 100 ppm Mo (Audétat 2019) and 100% precipitation efficiency of Mo from the fluids. Based on the outcrop area of intrusions and an assumed minimum thickness of 1 km, the constrained volume for the syn-mineralization intrusions in the Yangjiazhangzi deposit total less than 1 km^3 (Fig. 1d), which is significantly smaller than the minimum magma volume (i.e., 26 km^3) required for mineralization. On the contrary, the constrained volume for the cogenetic barren intrusions in the SYL ore zone is greater than 200 km^3 (Fig. 1b), large enough to produce a giant Mo deposit. The magma volume paradox outlined above indicates that the causative intrusions in porphyry Mo systems may solely act as conduits through which deep-seated magmas with fluid and molybdenum cargoes are transferred to the site of mineralization.

As shown in Figure 1 and Online Materials[1] Figure 1, the pre-mineralization intrusions in the arc-related SYL ore zone and Climax-type Hashitu deposit tend to occur as flat, ponded intrusions, whereas the cogenetic syn-mineralization intrusions typically occur as small stocks or dikes intruding into the pre-mineralization intrusions or wall rocks. Moreover, in areas where the syn-mineralization intrusion develops apophyses intruding into the pre-mineralization intrusion, molybdenite mineralization is generally well developed (Online Materials[1] Fig. 1). This arrangement indicates that the actual ore-forming event in porphyry Mo systems may be determined by spatial focusing of ore-forming fluids exsolved from the underlying magma chamber. If the fluids vent through flat, ponded intrusions, then the fluid flow may be insufficiently focused to lead to economic ore formation, as is considered the case for the Huangshan felsic pluton (Zhang and Audétat 2018) and the Yerington batholith (Schöpa et al. 2017). Instead, mineralization may only form when fluids are spatially focused along focusing structures, such as small igneous intrusive bodies. This inference is consistent with the geometries of the porphyry (-skarn) Mo deposits investigated in this and previous studies, which typically exhibit narrow cylindrical or pipe-like forms associated with small stocks or dikes with diameters of <500 m (e.g., Carten et al. 1993; Seedorff and Einaudi 2004; Gaynor et al. 2019; Ouyang et al. 2021; this study). The typical porphyritic texture of the syn-mineralization intrusions, as shown in Figure 2, suggests that draining magmas and fluids from an underlying magma chamber may be instantaneous (sudden), forceful, and voluminous. The rapid release of voluminous fluids has been shown to be key in the development of porphyritic textures (Nabelek et al. 2010). Such forceful discharge of voluminous fluids is also supported by the development of breccia pipes and stockwork mineralization in the deposits investigated in this study (Fig. 1e; Online Materials[1] Fig. 1) and in many other porphyry Mo deposits (e.g., Quartz Hill, Ashleman et al. 1997; Chalukou, Zhao et al. 2021; Luming, Ouyang et al. 2021). The field evidence presented above indicates that in porphyry Mo systems the forceful release of voluminous fluids, the formation of plug-shaped porphyritic intrusions, and focused fluid flow may be self-organizational and related. This is because once a steep pressure gradient develops in the upper part of a magma chamber, this site represents the most favorable location for the formation of focusing structures (e.g., plug-shaped intrusions) and voluminous venting of fluids (Castro and Dingwell 2009). Such self-organizational and related events are most likely related a sudden depressurization of the magma chamber as has been previously alluded to in the literature (e.g., Nishimura 2004; Castro and Dingwell 2009; Wotzlaw et al. 2014). Hence, we conclude that the sudden depressurization of the magma chamber and consequent venting of voluminous fluids along focusing structures (e.g., porphyry fingers) appears critical for the formation of porphyry Mo deposits of both arc-related and Climax-type. Determination of the processes responsible for the sudden depressurization of a magma chamber is beyond the scope of this study; however, notably, the most likely mechanisms include over-pressuring of a magma chamber by fluid exsolution during magmatic crystallization (e.g., Stock et al. 2016; Chelle-Michou et al. 2017), seismic shaking (e.g., Avouris et al. 2017), or a combination of the two (e.g., Nishimura 2004, 2017).

Implications for the exploration of porphyry Mo deposits

Existing hypotheses for the formation of porphyry Mo deposits broadly follow two distinct lines of argument. One view

is that specific magma sources or anomalously Mo-rich compositions are required to form economically significant porphyry Mo deposits (e.g., Pettke et al. 2010; Xie et al. 2017). In this scenario, parental magmas from the metasomatized mantle or lower crust are thought to be enriched in Mo from the outset. Empirical evidence for a source control includes the observation that some regions of the Earth, e.g., Colorado Mineral Belt of Western North America, Qinling-Dabie orogen of Central China, and northeastern China, seem particularly well endowed with porphyry Mo deposits. An alternative view, however, suggests that porphyry Mo mineralization is caused by specific magmas with normal Mo contents and elevated oxygen fugacity and water contents (e.g., Shu et al. 2019; Xing et al. 2021). If source characteristics are essential for the formation of porphyry Mo deposits, the potential of finding new mineral resources would be largely limited to specific provinces or regions. Alternatively, if specific magmas alone can account for the formation of porphyry Mo deposits, any area with suitable magmas (i.e., elevated oxygen fugacity and water content) could become a target for exploration.

The results presented in this study suggest that unique magma sources are not required for the formation of porphyry Mo deposits of both arc-related and Climax-type. Although the two classes of porphyry Mo deposits were formed in distinct tectonic settings and are associated with different kinds of intrusions, their formation is fundamentally controlled by similar geological processes and/or factors. A prerequisite for the formation of porphyry Mo deposits of both arc-related and Climax-type is the emplacement of oxidized, water-saturated magmas at 1.5 to 6.0 km palaeodepth. However, the actual ore-forming event itself is considered to relate to a sudden depressurization of the magma chamber and consequent venting of voluminous fluids along focusing structures, such as small stocks or dike swarms.

The tectonic setting and everything that relates to the evolution of the magma through to fluid saturation, emplacement of porphyries, and vein formation of the four selected deposits in this study are typical of the end-members of porphyry Mo family. As such, the conclusions of this work are potentially of utmost importance for exploration as they suggest fluid processes in the shallow crust are crucial for the formation of both arc-related and Climax-type porphyry Mo deposits. Meanwhile, we also infer that any area with a suitable magmatic-hydrothermal architecture could become a target for exploration of porphyry Mo deposits. Hence, it appears that the most important factor for the creation of porphyry deposits is the consolidation of an optimal combination of geometry, size, emplacement level, and particularly the roof shape of big granite plutons (i.e., magma chambers) that are coeval with mineralization. For these reasons, geophysical methods that relate directly to the geometry of magma chambers, such as seismic reflection and geomagnetic and gravity surveys, likely constitute the single most important tools in the uncovering of hidden porphyry deposits.

Acknowledgments and Funding

Constructive comments from three anonymous reviewers are greatly appreciated, together with the thorough editorial handling of associate editor Julie Roberge. This research is supported by National Key R&D Plan (Grant No. 2017YFC0601403), Scientific Research Fund of the China Central Non-Commercial Institute (No. KK2013), and International Postdoctoral Exchange Fellowship Program of China Postdoctoral Council (No. 20170032). We sincerely thank Detlef Krausse for help with the microprobe analyses and Raphael Njul for the excellent polishing work. We particularly thank Andreas Audétat for helping with sampling and melt inclusion LA-ICP-MS analyses.

References cited

Ashleman, J.C., Taylor, C.D., and Smith, P.R. (1997) Porphyry molybdenum deposits of Alaska, with emphasis on the geology of the Quartz Hill deposit, southeastern Alaska. Economic Geology, 9, 334–354.

Audétat, A. (2010) Source and evolution of molybdenum in the porphyry Mo (-Nb) deposit at Cave Peak, Texas. Journal of Petrology, 51, 1739–1760.

——— (2015) Compositional evolution and formation conditions of magmas and fluids related to porphyry Mo mineralization at Climax, Colorado. Journal of Petrology, 56, 1519–1546.

——— (2019) The metal content of magmatic-hydrothermal fluids and its relationship to mineralization potential. Economic Geology, 114, 1033–1056.

Audétat, A., and Li, W.T. (2017) The genesis of Climax-type porphyry Mo deposits, insights from fluid inclusions and melt inclusions. Ore Geology Reviews, 88, 436–460.

Audétat, A., Dolejs, D., and Lowenstern, J.B. (2011) Molybdenite saturation in silicic magmas, occurrence and petrological implications. Journal of Petrology, 52, 891–904.

Avouris, D.M., Carn, S.A., and Waite, G.P. (2017) Triggering of volcanic degassing by large earthquakes. Geology, 45, 715–718.

Ballard, J.R., Palin, M.J., and Campbell, I.H. (2002) Relative oxidation states of magmas inferred from Ce(IV)/Ce(III) in zircon: Application to porphyry copper deposits of northern Chile. Contributions to Mineralogy and Petrology, 144, 347–364.

Blichert-Toft, J., and Albarède, F. (1997) The Lu-Hf isotope geochemistry of chondrites and the evolution of the mantle-crust system. Earth and Planetary Science Letters, 148, 243–258.

Blichert-Toft, J., Chauvel, C., and Albarède, F. (1997) Separation of Hf and Lu for high-precision isotope analysis of rock samples by magnetic sector-multiple collector ICP-MS. Contributions to Mineralogy and Petrology, 127, 248–260.

Burnham, C.W. (1997) Magmas and hydrothermal fluids. In H.L. Barnes, Ed., Geochemistry of Hydrothermal Ore Deposits, 3rd ed., p. 63–122. Wiley.

Candela, P.A., and Bouton, S.L. (1990) The influence of oxygen fugacity on tungsten and molybdenum partitioning between silicate melts and ilmenite. Economic Geology, 85, 633–640.

Carten, R.B., White, W.H., and Stein, H.J. (1993) High-grade granite-related molybdenum systems: Classification and origin. In R.V. Kirkham, W.D. Sinclair, R.I. Thorpe, and J.M. Duke, Eds., Mineral Deposit Modeling, 40, p. 521–554. Geological Association of Canada, Special Paper.

Castro, J.M., and Dingwell, D.B. (2009) Rapid ascent of rhyolitic magma at Chaiten volcano, Chile. Nature, 461, 780–783.

Cerny, P., Blevin, P.L., Cuney, M., and London, D. (2005) Granite-related ore deposits. Society of Economic Geologists, 100, 337–370.

Chelle-Michou, C., Rottier, B., Caricchi, L., and Simpson, G. (2017) Tempo of magma degassing and the genesis of porphyry copper deposits. Scientific Reports, 7, 40566.

Chen, B., Zhai, M.G., and Tian, W. (2007) Origin of the Mesozoic magmatism in the North China Craton, constraints from petrological and geochemical data. Geological Society, London, Special Publications, 280, 131–151.

Chen, Y.J., Zhang, C., Wang, P., Pirajno, F., and Li, N. (2017) The Mo deposits of northeast China: a powerful indicator of tectonic settings and associated evolutionary trends. Ore Geology Reviews, 81, 602–640.

Chu, S.X., Zeng, Q.D., and Liu, J.M. (2017) Re-Os and U-Pb geochronology of the Songbei porphyry-skarn Mo deposit, North China Craton, Implications for the Early Jurassic tectonic setting in eastern China. Journal of Geochemical Exploration, 181, 256–269.

Cui, Y.B. (2019) Study on buried granite and its contact metamorphism in Yangjiazhangzi, Western Liaoning Province. Jiling University, 45.

Dai, J.Z., Mao, J.W., Zhao, C.S., Li, F.R., Wang, R.T., Xie, G.Q., and Yang, F.Q. (2008) Zircon SHRIMP U-Pb age and petrogeochemical features of Lianjiagou granite in western Liaoning province. Acta Geologica Sinica, 82, 1555–1564 (in Chinese with English abstract).

Devine, J.D., Gardner, J.E., Brack, H.P., Layne, G.D., and Rutherford, M.J. (1995) Comparison of microanalytical methods for estimating H_2O contents of silicic volcanic glasses. American Mineralogist, 80, 319–328.

Dilles, J.H. (1987) Petrology of the Yerington batholith, Nevada: Evidence for evolution of porphyry copper ore fluids. Economic Geology, 82, 1750–1789.

Ding, C.W., Dai, P., Bagas, L., Nie, F.J., Jiang, S.H., Wei, J.H., Ding, C.Z., Zuo, P.F., and Zhang, K. (2016) Geochemistry and Sr-Nd-Pb isotopes of the granites from the Hashitu Mo deposit of Inner Mongolia, China: Constraints on their origin and tectonic setting. Acta Geologica Sinica (English Edition), 90, 106–120.

Dingwell, D.B., Scarfe, M.C., and Cronin, D.J. (1985) The effect of fluorine on viscosities in the system Na_2O-Al_2O_3-SiO_2: Implications for phonolites, trachytes and rhyolites. American Mineralogist, 70, 80–87.

Donovan, J., and Vicenzi, E. (2008) Water by EPMA-new developments. Microscopy and Microanalysis, 14, 1274–1275.

Fountain, D.M., and Christensen, N.I. (1989) Composition of the continental crust

and upper mantle: A review. Geophysical Framework of the Continental United States, 172, 711–742.
Gaynor, S.P., Rosera, J.M., and Coleman, D.S. (2019) Intrusive history of the Oligocene Questa porphyry molybdenum deposit, New Mexico. Geosphere, 15, 548–575.
Ge, W.C., Wu, F.Y., Zhou, C.Y., and Zhang, J.H. (2007) Porphyry Cu-Mo deposits in the eastern Xing'an-Mongolian orogenic belt: Mineralization ages and their geodynamic implications. Chinese Science Bulletin, 52, 3416–3427.
Goldfarb, R.J., Mao, J.W., Qiu, K.F., and Goryachev, N. (2021) The great Yanshanian metallogenic event of eastern Asia: Consequences from one hundred million years of plate margin geodynamics. Gondwana Research, 100, 223–250.
Griffin, W.L., Pearson, N.J., Belousova, E., Jackson, S.E., Van Achterbergh, E., O'Reilly, S.Y., and Shee, S.R. (2000) The Hf isotope composition of cratonic mantle, LAM-MC-ICPMS analysis of zircon megacrysts in kimberlites. Geochimica et Cosmochimica Acta, 64, 133–147.
Griffin, W.L., Wang, X., Jackson, S.E., Pearson, N., O'Reilly, S.Y., Xu, X.S., and Zhou, X.M. (2002) Zircon chemistry and magma mixing, SE China, in-situ analysis of Hf isotopes. Lithos, 61, 237–269.
Han, C.M., Xiao, W.J., Zhao, G.C., Sun, M., Qu, W.J., and Du, A.D. (2009) A Re-Os study of molybdenites from the Lanjiagou Mo deposit of North China Craton and its geological significance. Gondwana Research, 16, 264–271.
Hayden, L.A., and Watson, B.E. (2007) Rutile saturation in hydrous siliceous melts and its bearing on Ti-thermometry of quartz and zircon. Earth and Planetary Science Letters, 258, 561–568.
Holtz, F., Johannes, W., Tamic, N., and Behrens, H. (2001) Maximum and minimum water contents of granitic melts generated in the crust: A reevaluation and implications. Lithos, 56, 1–14.
Huang, R., and Audétat, A. (2012) The titanium-in-quartz (TitaniQ) thermobarometer: A critical examination and re-calibration. Geochimica et Cosmochimica Acta, 84, 75–89.
Huang, D.H., Dong, Q.Y., and Gan, Z.X. (1989) China molybdenum deposits. In S.H. Song Eds., China Deposits, 1, pp, 493–536. Geology Publishing House. (in Chinese)
Huang, D.H., Wu, C.Y., Du, A.D., and He, H.L. (1994) Re-Os ages molybdenum deposits in east Qinling and their significance. Mineral Deposits, 13, 221–230 (in Chinese).
Irvine, T.N.J., and Baragar, W.R.A. (1971) A guide to the chemical classification of the common volcanic rocks. Canadian Journal of Earth Sciences, 8, 523–548.
Ishihara, S., and Shibata, K. (1980) Mineralization age of the Yangjiazhangzi molybdenum deposits. China. Mining Geology, 30, 27–29.
Jiang, N., Zhang, S.Q., Zhou, W., and Liu, Y.S. (2009) Origin of a Mesozoic granite with A-type characteristics from the North China craton: Highly fractionated from I-type magmas? Contributions to Mineralogy and Petrology, 158, 113–130.
Johannes, W., and Holtz, F. (1996) Petrogenesis and experimental Petrology of Granitic Rocks, 335 p. Springer.
Keith, J.D., Christiansen, E.H., and Carten, R.B. (1993) The genesis of giant porphyry molybdenum deposits. In B.H. Whiting, C.J. Hodgson, and R. Mason, Eds., Giant Ore Deposits, p. 285–317. Society of Economic Geologists.
Keppler, H., and Wyllie, P.J. (1991) Partitioning of Cu, Sn, Mo, W, U, and Th between melt and aqueous fluid in the systems haplogranite-H_2O-HCl and haplogranite-H_2O-HF. Contributions to Mineralogy and Petrology, 109, 139–150.
Kularatne, K., and Audétat, A. (2014) Rutile solubility in hydrous rhyolite melts at 750–900°C and 2 kbar, with application to titanium-in-quartz (TitaniQ) thermobarometry. Geochimica et Cosmochimica Acta, 125, 196–209.
Le Bas, M.J., Maitre, R.W.L., Streckeisen, A., Zanettin, B., and IUGS Subcommission on the Systematics of Igneous Rocks. (1986) A chemical classification of volcanic rocks based on the total alkali-silica diagram. Journal of Petrology, 27, 745–750.
Lerchbaumer, L., and Audétat, A. (2013) The metal content of silicate melts and aqueous fluids in subeconomically Mo mineralized granites: Implications for porphyry Mo genesis. Economic Geology, 108, 987–1013.
Liu, J.F., Li, J.Y., Chi, X.G., Zheng, P.X., Hu, Z.C., and Zhang, X.W. (2020) Destruction of the northern nargin of the North China Craton in Mid-Late Triassic: Evidence from asthenosphere-derived mafic enclaves in the Jiefangyingzi granitic pluton from the Chifeng area, southern Inner Mongolia. Acta Geologica Sinica, 94, 1071–1092 (English edition).
Lowenstern, J.B. (1994) Dissolved volatile concentrations in an ore-forming magma. Geology, 22, 893–896.
Ludington, S., and Plumlee, G.S. (2009) Climax-type porphyry molybdenum deposits, 16 p. U.S. Geological Survey.
McCulloch, M.T., Rosman, K.J., and De Laeter, J.R. (1977) The isotopic and elemental abundance of ytterbium in meteorites and terrestrial samples. Geochimica et Cosmochimica Acta, 41, 1703–1707.
Meng, Q.R. (2003) What drove late Mesozoic extension of the northern China-Mongolia tract? Tectonophysics, 369, 155–174.
Nabelek, P.I., Whittington, A.G., and Sirbescu, M.L.C. (2010) The role of H_2O in rapid emplacement and crystallization of granite pegmatites, resolving the paradox of large crystals in highly undercooled melts. Contributions to Mineralogy and Petrology, 160, 313–325.
Nishimura, T. (2004) Pressure recovery in magma due to bubble growth. Geophysical Research Letters, 31.
——— (2017) Triggering of volcanic eruptions by large earthquakes. Geophysical Research Letters, 44, 7750–7756.
Ouyang, H.G., Mao, J.W., Santosh, M., Zhou, J., Zhou, Z.H., Wu, Y., and Hou, L. (2013) Geodynamic setting of Mesozoic magmatism in NE China and surrounding regions, perspectives from spatio-temporal distribution patterns of ore deposits. Journal of Asian Earth Sciences, 78, 222–236.
Ouyang, H.G., Mao, J.W., and Hu, R.Z. (2020) Geochemistry and crystallization conditions of magmas related to porphyry Mo mineralization in northeastern China. Economic Geology, 115, 79–100.
Ouyang, H.G., Mao, J.W., Hu, R.Z., Caulfield, J., and Zhou, Z.H. (2021) Controls on the metal endowment of porphyry Mo deposits: Insights from the Luming porphyry Mo deposit, northeastern China. Economic Geology, 116, 1711–1735.
Pettke, T., Oberli, F., and Heinrich, C.A. (2010) The magma and metal source of giant porphyry-type ore deposits, based on lead isotope microanalysis of individual fluid inclusions. Earth and Planetary Science Letters, 296, 267–277.
Richards, J.P. (2011a) Magmatic to hydrothermal metal fluxes in convergent and collided margins. Ore Geology Reviews, 40, 1–26.
——— (2011b) High Sr/Y arc magmas and porphyry Cu±Mo±Au deposits: Just add water. Economic Geology, 106, 1075–1081.
Romick, J.D., Kay, S.M., and Kay, R.W. (1992) The influence of amphibole fractionation on the evolution of calc-alkaline andesite and dacite tephra from the central Aleutians, Alaska. Contributions to Mineralogy and Petrology, 112, 101–118.
Schöpa, A., Annen, C., Dilles, J.H., Sparks, R.S.J., and Blundy, J.D. (2017) Magma emplacement rates and porphyry copper deposits: Thermal modeling of the Yerington Batholith, Nevada. Economic Geology, 112, 1653–1672.
Seedorff, E., and Einaudi, M.T. (2004) Henderson porphyry molybdenum system, Colorado, I. Sequence and abundance of hydrothermal mineral assemblages, flow paths of evolving fluids, and evolutionary style. Economic Geology, 99, 3–37.
Seedorff, E., Dilles, J.H., Proffett, J.M. Jr., Einaudi, M.R., Zurcher, L., Stavast, W.J.A., Johnson, D.A., and Barton, M.D. (2005) Porphyry copper deposits: Characteristics and origin of hypogene features. In J.W. Hedenquist, J.F.H. Thompson, R.J. Goldfarb, and J.P. Richards, Eds., Economic Geology and Bulletin of the Society of Economic Geologists One Hundredth Anniversary Volume 1905–2005, p. 251–298. Society of Economic Geologists, Littleton, Colorado.
Shu, Q.H., and Chiaradia, M. (2021) Mesozoic Mo mineralization in northeastern China did not require regional-scale pre-enrichment. Economic Geology, 116, 1227–1237.
Shu, Q.H., Chang, Z.S., Lai, Y., Zhou, Y.T., Sun, Y., and Yan, C. (2016) Regional metallogeny of Mo-bearing deposits in northeastern China, with new Re-Os dates of porphyry Mo deposits in the northern Xilamulun district. Economic Geology, 111, 1783–1798.
Shu, Q.H., Chang, Z.S., Lai, Y., Hu, X., Wu, H., Zhang, Y., Wang, P., Zhai, D.G., and Zhang, C. (2019) Zircon trace elements and magma fertility, insights from porphyry (-skarn) Mo deposits in NE China. Mineralium Deposita, 54, 645–656.
Sláma, J., Košler, J., Condon, D.J., Crowley, J.L., Gerdes, A., Hanchar, J.M., Horstwood, M.S.A., Morris, G.A., Nasdala, L., Norberg, N., Schaltegger, U., Schoene, B., Tubrett, M.N., and Whitehouse, M.J. (2008) Plešovice zircon-a new natural reference material for U-Pb and Hf isotopic microanalysis. Chemical Geology, 249, 1–35.
Söderlund, U., Patchett, P.J., Vervoort, J.D., and Isachsen, C.E. (2004) The ^{176}Lu decay constant determined by Lu-Hf and U-Pb isotope systematics of Precambrian mafic intrusions. Earth and Planetary Science Letters, 219, 311–324.
Stein, H.J., and Hannah, J.L. (1985) Movement and origin of ore fluids in Climax-type systems. Geology, 13, 469–474.
Stock, M.J., Humphreys, M.C., Smith, V.C., Isaia, R., and Pyle, D.M. (2016) Late-stage volatile saturation as a potential trigger for explosive volcanic eruptions. Nature Geoscience, 9, 249–254.
Sun, S.S., and McDonough, W.F. (1989) Chemical and isotopic systematics of oceanic basalts, implications for mantle composition and processes. Geological Society, London, Special Publications, 42, 313–345.
Taylor, R.D., Hammarstrom, J.M., Piatak, N.M., and Seal, R.R. (2012) Arc-related porphyry molybdenum deposit model, 64 p. U.S. Geological Survey.
Watson, B.E., and Harrison, M.T. (1983) Zircon saturation revisited: temperature and composition effects in a variety of crystal magma types. Earth and Planetary Science Letters, 64, 295–304.
Webster, J.D. (1997) Chloride solubility in felsic melts and the role of chloride in magmatic degassing. Journal of Petrology, 38, 1793–1807.
Whalen, J.B., Currie, K.L., and Chappell, B.W. (1987) A-type granites, geochemical characteristics, discrimination and petrogenesis. Contributions to Mineralogy and Petrology, 95, 407–419.
Whalen, J.B., Anderson, R.G., Struik, L.C., and Villeneuve, M.E. (2001) Geochemistry and Nd isotopes of the François Lake plutonic suite, Endako batholith, host and progenitor to the Endako molybdenum camp, central British Columbia.

Canadian Journal of Earth Sciences, 38, 603–618.
White, W.H., Bookstrom, A.A., Kamilli, R.J., Ganster, M.W., Smith, R.P., and Ranta, D.E., and Steininger, R.C. (1981) Character and origin of Climax-type molybdenum deposits. Economic Geology, 270–316. 75th Anniversary Volume.
Windley, B.F., Alexeiev, D., Xiao, W., Kröner, A., and Badarch, G. (2007) Tectonic models for accretion of the Central Asian Orogenic Belt. Journal of the Geological Society, 164, 31–47.
Wotzlaw, J.F., Bindeman, I.N., Watts, K.E., Schmitt, A.K., Caricchi, L., and Schaltegger, U. (2014) Linking rapid magma reservoir assembly and eruption trigger mechanisms at evolved Yellowstone-type supervolcanoes. Geology, 42, 807–810.
Wu, L.R., Zhang, X.Q., and Sun, S.H. (1990) On the magma generation, evolution and molybdenum mineralization of the Yangjiazhangzi complex, Jinxi, Liaoning province. Acta Petrologica Sinica, 3, 1–11 (in Chinese).
Wu, F.Y., Sun, D.Y., Li, H.M., Jahn, B.M., and Wilde, S. (2002) A-type granites in northeastern China: Age and geochemical constraints on their petrogenesis. Chemical Geology, 187, 143–173.
Wu, F.Y., Jahn, B.M., Wilde, S.A., Lo, C.H., Yui, T.F., Lin, Q., Ge, W.C., and Sun, D.Y. (2003) Highly fractionated I-type granites in NE China (II): Isotopic geochemistry and implications for crustal growth in the Phanerozoic. Lithos, 67, 191–204.
Wu, F.Y., Lin, J.Q., Wilde, S.A., Zhang, X.O., and Yang, J.H. (2005) Nature and significance of the Early Cretaceous giant igneous event in eastern China. Earth and Planetary Science Letters, 233, 103–119.
Wu, F.Y., Yang, J.H., Zhang, H.B., and Liu, X.M. (2006) Emplacement ages of the Mesozoic granites in southeastern part of the Western Liaoning Province. Acta Petrological Sinica, 22, 315–325.
Wu, F.Y., Sun, D.Y., Ge, W.C., Zhang, Y.B., Grant, M.L., Wilde, S.A., and Jahn, B.M. (2011) Geochronology of the Phanerozoic granitoids in northeastern China. Journal of Asian Earth Sciences, 41, 1–30.
Wu, F.Y., Liu, X.C., Ji, W.Q., Wang, J.M., and Yang, L. (2017) Highly fractionated granites: Recognition and research. Science China Earth Sciences, 60, 1201–1219.
Xiao, W.J., Windley, B.F., Hao, J., and Zhai, M.G. (2003) Accretion leading to collision and the Permian Solonker suture, Inner Mongolia, China, termination of the central Asian orogenic belt. Tectonics, 22, 1069, doi:10.1029/2002TC001484.
Xie, G.Q., Mao, J.W., Wang, R.T., Meng, D.M., Sun, J., Dai, J.Z., Ren, T., Li, J.B., and Zhao, H.J. (2017) Origin of the Lengshuigou porphyry-skarn Cu deposit in the Zha-Shan district, South Qinling, central China, and implications for differences between porphyry Cu and Mo deposits. Mineralium Deposita, 52, 621–639.
Xing, K., Shu, Q.H., and Lentz, D.R. (2021) Constraints on the formation of the giant Daheishan porphyry Mo deposit (NE China) from whole-rock and accessory mineral geochemistry. Journal of Petrology, 62.
Xu, W.L., Gao, S., Wang, Q.H., Wang, D.Y., and Liu, Y.S. (2006) Mesozoic crustal thickening of the eastern North China craton: Evidence from eclogite xenoliths and petrologic implications. Geology, 34, 721–724.
Xu, W.-L., Pei, F.-P., Wang, F., Meng, E., Ji, W.-Q., Yang, D.-B., and Wang, W. (2013) Spatial-temporal relationships of Mesozoic volcanic rocks in NE China, constraints on tectonic overprinting and transformations between multiple tectonic regimes. Journal of Asian Earth Sciences, 74, 167–193.
Xu, X.C., Zhang, X.X., Zheng, C.Q., Cui, F.H., Gao, Y., and Gao, F. (2015) Geochemistry and chronology characteristics of the intrusive rocks and its relationship with mineralization in Yangjiazhangzi area, western Laioning province. Journal of Jilin University, 45, 804–819 (in Chinese with English abstract).
Yuan, H.L., Gao, S., Dai, M.N., Zong, C.L., Günther, D., Fontaine, G.H., Liu, X.M., and Diwu, C.R. (2008) Simultaneous determinations of U-Pb age, Hf isotopes and trace element compositions of zircon by excimer laser-ablation quadrupole and multiple-collector ICP-MS. Chemical Geology, 247, 100–118.
Zeng, Q.D., Liu, J.M., Qin, K.Z., Fan, H.R., Chu, S.X., Wang, Y.B., and Zhou, L.L. (2013) Types, characteristics, and time-space distribution of molybdenum deposits in China. International Geology Review, 55, 1311–1358.
Zhai, D.G., Liu, J.J., Wang, J.P., Yang, Y.Q., Zhang, H.Y., Wang, X.L., Zhang, Q.B., Wang, G.W., and Liu, Z.J. (2014) Zircon U-Pb and molybdenite Re-Os geochronology, and whole-rock geochemistry of the Hashitu molybdenum deposit and host granitoids, Inner Mongolia, NE China. Journal of Asian Earth Sciences, 79, 144–160.
Zhai, D.G., Liu, J.J., Tombros, S., and Williams-Jones, A.E. (2018) The genesis of the Hashitu porphyry molybdenum deposit, Inner Mongolia, NE China, constraints from mineralogical, fluid inclusion, and multiple isotope (H, O, S, Mo, Pb) studies. Mineralium Deposita, 53, 377–397.
Zhang, D.H., and Audétat, A. (2017) Chemistry, mineralogy and crystallization conditions of porphyry Mo-forming magmas at Urad-Henderson and Silver Creek, Colorado, U.S.A. Journal of Petrology, 58, 277–296.
——— (2018) Magmatic-hydrothermal evolution of the barren Huangshan pluton, Anhui province, China: A melt and fluid inclusion study. Economic Geology, 113, 803–824.
Zhang, K., Nie, F.J., Hou, W.R., Li, C., and Liu, Y. (2012) Re-Os isotopic age dating of molybdenite separates from Hashitu Mo deposit in Linxi County of Inner Mongolia and its geological significance. Mineral Deposits, 31, 129–138.
Zhang, S.H., Zhao, Y., Davis, G.A., Ye, H., and Wu, F. (2014) Temporal and spatial variations of Mesozoic magmatism and deformation in the North China craton: Implications for lithospheric thinning and decratonization. Earth-Science Reviews, 131, 49–87.
Zhang, Q., Liang, C.Y., Liu, Y.J., Zheng, C.Q., and Li, W.M. (2019) Final closure time of the Paleo-Asian Ocean: Implication from the provenance transformation from the Yangjiagou Formation to Lujiatun Formation in the Jiutai area, NE China. Acta Geologica Sinica, English Edition, 93, 1456–1476.
Zhao, Q.Q., Zhai, D.G., Mathur, R., Liu, J.J., Selby, D., and Williams-Jones, A.E. (2021) The giant Chalukou porphyry Mo deposit, northeast China: The product of a short-lived, high flux mineralizing event. Economic Geology, 116, 1209–1225.
Zheng, Y.C., Feng, H., Wu, C.Z., Gu, L.X., Liu, S.H., and He, K. (2014) Influence of crude oil on the genesis of the Lanjiagou porphyry molybdenum deposit, western Liaoning Province, China. Ore Geology Reviews, 60, 1–13.

Manuscript received June 11, 2020
Manuscript accepted August 26, 2021
Manuscript handled by Julie Roberge

Endnote:

[1]Deposit item AM-22-97665, Online Materials. Deposit items are free to all readers and found on the MSA website, via the specific issue's Table of Contents (go to http://www.minsocam.org/MSA/AmMin/TOC/2022/Sep2022_data/Sep2022_data.html).